

The Whittle Likelihood for Complex-Valued Time Series

Adam M. Sykulski, Sofia C. Olhede, Jonathan M. Lilly and Jeffrey J. Early

Abstract

This paper introduces a version of the Whittle likelihood for complex-valued processes. This represents a nontrivial extension of the Whittle likelihood for bivariate real-valued processes, as complex-valued models can capture structure that is only evident by separating negative and positive frequency behaviour. Flexible inference methods for such parametric models are proposed, and the properties of such methods are derived. The methods are applied to oceanographic time series, as a naturally occurring sampled complex-valued time process. We demonstrate how to reduce estimation bias and ameliorate sampling effects semi-parametrically, thus advancing the state-of-the-art in frequency domain modelling and estimation of time series in general. We test the hypothesis that the negative and positive frequency behaviour of the process are independent, or equivalently that the process is isotropic or proper, and show the performance of the methodology on simulated and real-world data.

Keywords: Sampled continuous-time processes; Rotary and Cartesian components; Discrete Fourier Transform; Periodogram; Semi-parametric; Matérn process; Propriety; Anisotropy.

1 Introduction

This paper develops new models for bivariate (or complex-valued) time series. We derive the interpretation of such models, and efficient methods for their estimation, based on sampled time series. Complex-valued time series arise in a number of important application areas, for example functional magnetic resonance imaging (Rowe, 2005), blood-flow observations (Olhede and Walden, 2003) and climate time series in oceanography (Griffa et al., 2007; LaCasce, 2008). A number of recent advances in methodological statistics for the analysis of complex-valued vectors, as well as for time-series samples (Rubin-Delanchy and Walden, 2008; Walden, 2013; Schreier and Scharf, 2010), have been developed with the motivation of such data sets. Approaches have mainly been non-parametric, and little focus has been placed on methods for efficient parametric inference. Our approach to parametric modelling is based on frequency domain understanding, and we aim to adapt the Whittle likelihood (Whittle, 1953b; Dzhaparidze and Yaglom, 1983) to this end.

To show the relevance of our work to practice, we plot observations from the Global Drifter Program (GDP, <http://www.aoml.noaa.gov/phod/dac>) in the first panel of Figure 1. The GDP is a unique database of global circulation measurements which impacts our understanding of decadal to century-scale climate change. Each series in this data set is a complex-valued series, and we show a plot of locations from a single series in the top right of Figure 1. The velocities in each Cartesian component, and the magnitude square of the Fourier transform of the complex-valued velocities (for the first quarter of the series), are displayed on the bottom row of Figure 1. We have plotted the negative and positive frequency axes overlain, and it is clear that certain features are only present on one side of the spectrum. The frequency-domain content of this complex-valued process is much simpler to capture than the time-domain content of the real-valued bivariate process. This motivates us to properly formulate the modelling and inference of processes with such non-Hermitian structure. The main aim of this paper is to develop understanding of such models, and a complete picture of what properties spectral inference methods possess in this context.

Adam M. Sykulski and Sofia C. Olhede are with the Department of Statistical Science, University College London, Gower Street, London WC1 E6BT, UK (a.sykulski@ucl.ac.uk, s.olhede@ucl.ac.uk), tel: +44 20 7679 1872, fax: +44 20 3108 3105.

Jonathan M. Lilly and Jeffrey J. Early are with Northwest Research Associates, PO Box 3027, Bellevue, WA 98009-3027, USA (lilly@nwra.com, jearly@nwra.com), tel: +1 425 556 9055, fax: +1 425 556 9099.

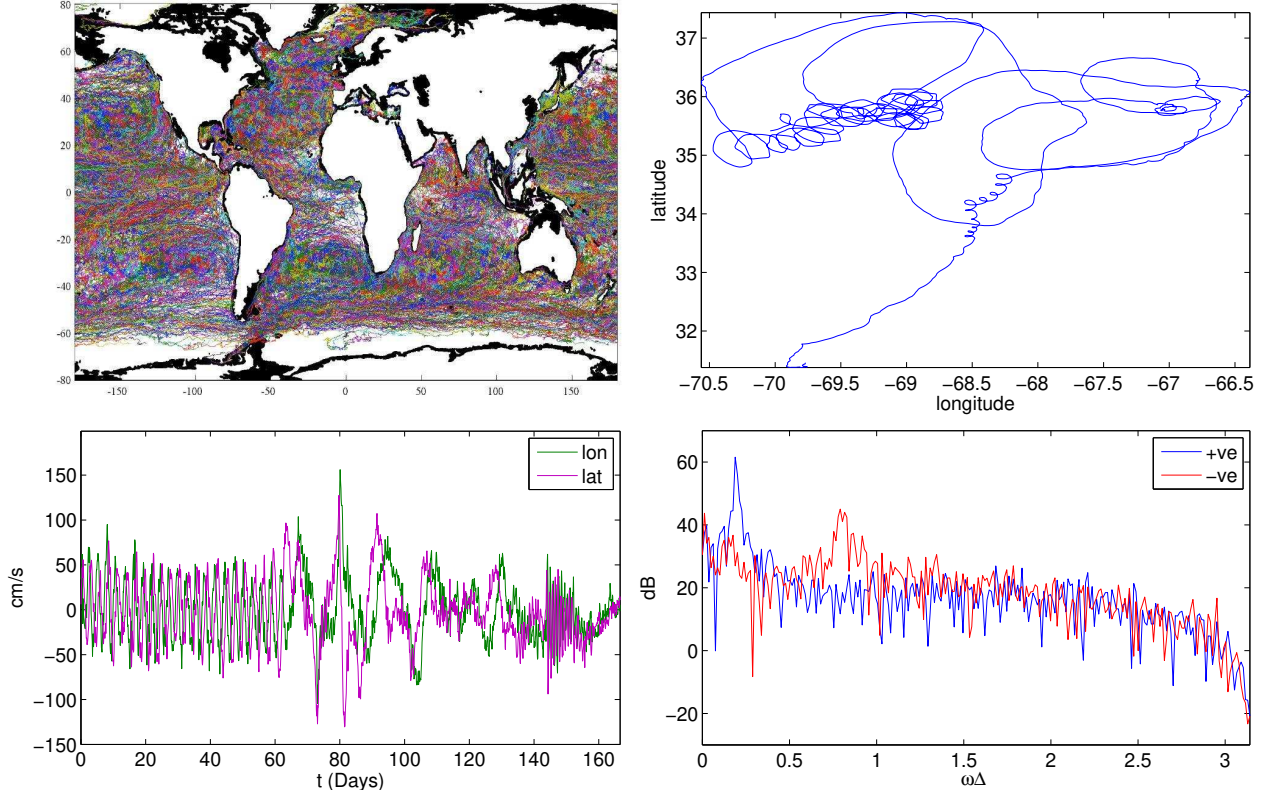


Figure 1: (Top-left) Trajectories from the Global Drifter Program. (Top-right) A 167 day trajectory of a North-Atlantic drifter. (Bottom-left) velocities of this drifter over time in each Cartesian direction. (Bottom-right) the estimated power spectrum of the complex-valued velocities (first 40 days only).

The second aim of this paper is to practically and efficiently adapt Whittle likelihood for sampled processes. For asymptotic understanding, well-established results have been the consequence of the initially derived theory, e.g. Whittle (1953b); Dzhaparidze and Yaglom (1983). For finite N , more subtle effects are known to be in evidence, see also Dahlhaus (1988). Small sample effects are particularly important as the time series we shall observe experience potential time-variation in the process' generating mechanism (as in Figure 1), which will limit the length of time series we can perform analysis of simultaneously. We shall implement Fourier domain analysis, and use stationary models, but implicitly will assume that such analyses will be time-limited.

We shall also address a number of more complicated effects. These are due to the nature of discrete sampling mechanisms of continuous time processes, that we inevitably observe as discrete time samples. We refer to our approach as “semi-parametric”, as we cannot directly model, in closed form, all effects that are expressed in the data. We aim to unify ideas of frequency domain misfit related to high frequency nuisance structure (Robinson, 1995), apparent in particular in our application due to interpolation (Hansen and Poulain, 1996), and the effects of time-variation (Van Bellegem and Dahlhaus, 2006). Our aim is to respect the constraints of computational tractability, especially important for analysing large volumes of long-duration time series. As our methods must be implementable on the full GDP data set, we aim to handle large data volumes, with potentially extremely heterogeneous structure.

At first glance, it may seem that formulating the theory and methods of complex-valued time series, is just a special case of the study of bivariate and real-valued time series, as linear relationships relate real-valued processes to their complex representation. This is *not* the case, due to the widely linear transformation between the real and imaginary part of the series, and the series itself, having a special impact

on the Fourier representation of the process. Rotary structure, e.g. the relationship between negative and positive frequencies, can easily be specified in the complex plane, but is hard to parameterise when handling real-valued processes. The proposed models will be formulated as complex-valued, but will lead to new forms of interpretable real-valued structure, easily relatable to multivariate families (Gneiting et al., 2010; Apanasovich et al., 2012). The classes will yield new insights into our understanding of bivariate real-valued structure also, a fact we shall explore further.

The paper is organised as follows. In Section 2 we provide some necessary preliminaries on real- and complex-valued time series. In Section 3 we introduce our models for Cartesian and rotary structure in complex-valued time series and extend the Matérn process to the complex-plane. Section 4 introduces the Whittle likelihood for complex-valued time series and also the *blurred* likelihood which correctly accounts for finite-sample bias in both real- and complex-valued time series. We then discuss relevant properties in Section 5. In Section 6 we provide a guide on inference procedures including semi-parametric inference, likelihood ratio tests and model choice. Finally, in Section 7 we demonstrate our various modelling and inference procedures, including a detailed analysis of oceanographic flow data. Concluding remarks and future work can be found in Section 8.

2 Preliminaries

2.1 Real-valued Time Series

We denote the sequence $\{X_t\}_{t=1}^N$ as X and assume it is a regularly-sampled zero-mean continuous Gaussian process fully specified by its covariance $c_{XX}(t_1, t_2) = \text{Cov}\{X_{t_1}, X_{t_2}\} = \mathbb{E}\{X_{t_1}X_{t_2}\}$, where $X_t = X(t\Delta)$ and Δ is the sampling period. For stationary processes we define the autocovariance sequence $s_{XX}(|t_1 - t_2|) = c_{XX}(t_1, t_2)$ ($1 \leq t_1, t_2 \leq N$). The power spectral density forms a Fourier pair with the autocovariance sequence:

$$S_{XX}(\omega) = \Delta \sum_{\tau=-\infty}^{\infty} s_{XX}(\tau)e^{-i\omega\tau\Delta}, \quad s_{XX}(\tau) = \frac{1}{2\pi} \int_{-\pi/\Delta}^{\pi/\Delta} S_{XX}(\omega)e^{i\omega\tau\Delta}d\omega. \quad (2.1)$$

Here the angular frequency $\omega \in [-\pi/\Delta, \pi/\Delta]$ is given in radians. A first (inconsistent) estimate of $S_{XX}(\omega)$ corresponds to the periodogram (denoted $\hat{S}_{XX}(\omega)$), which is the squared absolute value of the Discrete Fourier Transform (DFT, denoted $J_X(\omega)$) given by

$$J_X(\omega) = \sqrt{\frac{\Delta}{N}} \sum_{t=1}^N X_t e^{-i\omega t\Delta}, \quad \hat{S}_{XX}(\omega) = |J_X(\omega)|^2, \quad \omega = \frac{2\pi}{N\Delta} \left(1 - \lceil \frac{N}{2} \rceil, \dots, \lfloor \frac{N}{2} \rfloor\right). \quad (2.2)$$

Using the spectral representation theorem we can write X in terms of orthogonal increments

$$X_t = \frac{1}{2\pi} \int_{-\pi/\Delta}^{\pi/\Delta} d\Psi_X(\omega)e^{i\omega t\Delta}, \quad (2.3)$$

where $\text{var}(d\Psi_X(\omega)) = S_{XX}(\omega)d\omega$. Note that because X_t is the sampled process, $d\Psi_X(\omega)$ has already been aliased. There is an analogue to equation (2.3) which is valid for the continuous-time process $X(t)$. Finally, as X is real-valued, it is generally understood from half of its frequencies (i.e. any given half is redundant). We can write

$$X_t = \frac{1}{2\pi} \int_{-\pi/\Delta}^0 d\Psi_X(\omega)e^{i\omega t\Delta} + \frac{1}{2\pi} \int_0^{\pi/\Delta} d\Psi_X(\omega)e^{i\omega t\Delta} = (X_t^-)^* + X_t^+. \quad (2.4)$$

We call X^- and X^+ the *rotary components* of X . As X is real-valued, it follows that $X^- \equiv X^+$ because of our choice of conjugation of X^- . The decomposition into X_t^+ and X_t^- may seem alien, but normally when we analyse the spectral information of X_t this decomposition is made implicitly.

A direct consequence of equations (2.2) and (2.3) is that by calculating the DFT from a finite sample size, we have “blurred” the spectral information. For this reason the periodogram is a naïve estimate of the spectral density, as it is equal to the convolution of the true spectrum with the Fejér kernel (the magnitude-squared of the Dirichlet kernel). This convolution can cause badly biased spectral estimates (Percival and Walden, 1993). Such effects are often tackled by using tapering (Velasco and Robinson, 2000) which reduces leakage at the expense of increased correlation between neighbouring Fourier frequencies – the periodogram may therefore still be a preferable estimate for certain processes. There is also the issue of aliasing, which results in energy outside of the Nyquist frequency (the highest observable frequency) being folded back into the observable spectrum, which is often ignored when considering the estimation of spectra of continuous sampled processes (Percival and Walden, 2006). In Section 4 we propose new methodology for inference via the Whittle likelihood, by efficiently incorporating these finite sampling effects correctly, which can be used with either the periodogram or tapered spectral estimates.

2.2 Complex-valued Time Series

We shall motivate our methodological advances by problems in oceanography. The analysis of complex-valued time series has been addressed in oceanography since Gonella (1972). Here the real and imaginary parts of the complex-valued series are referred to as the *Cartesian components*, but it is more convenient to model them as *rotary components*, or as an aggregation of processes supported only on negative or positive frequencies (Walden, 2013), such as X_t^- and X_t^+ in equation (2.4).

To form a complex-valued series, we start from a bivariate real series, X_t and Y_t . These processes can be combined to form the complex-valued process Z via $Z_t = X_t + iY_t$. We shall assume that X and Y are jointly Gaussian, such that any collection of the processes at a number of sampled points are Gaussian. Therefore to fully characterise their properties we need to specify the joint covariance $c_{XY}(t_1, t_2) = \text{Cov}\{X_{t_1}, Y_{t_2}\} = \mathbb{E}\{X_{t_1}Y_{t_2}\}$ as well as $c_{XX}(t_1, t_2)$ and $c_{YY}(t_1, t_2)$. If the process is stationary then $c_{XY}(t_1, t_2) = s_{XY}(\tau)$ (where $\tau = |t_1 - t_2|$) and the cross-spectrum $S_{XY}(\omega)$ forms a Fourier pair with $s_{XY}(\tau)$, as in equation (2.1). In terms of the complex-valued process Z , the stationary process is fully characterised by specifying the covariance and *relation* sequence $r_{ZZ}(\tau)$

$$\begin{aligned} s_{ZZ}(\tau) &= \mathbb{E}\{Z_t Z_{t+\tau}^*\} = s_{XX}(\tau) + s_{YY}(\tau) + i[s_{XY}(-\tau) - s_{XY}(\tau)], \\ r_{ZZ}(\tau) &= \mathbb{E}\{Z_t Z_{t+\tau}\} = s_{XX}(\tau) - s_{YY}(\tau) + i[s_{XY}(-\tau) + s_{XY}(\tau)], \end{aligned} \quad (2.5)$$

with Z_t^* denoting the complex conjugate of Z_t . Once we have specified $s_{ZZ}(\tau)$ and $r_{ZZ}(\tau)$, the full joint covariance structure of X_t and Y_t are specified, as we can recover $\{s_{XX}(\tau)\}$, $\{s_{YY}(\tau)\}$ and $\{s_{XY}(\tau)\}$ from $\{s_{ZZ}(\tau)\}$ and $\{r_{ZZ}(\tau)\}$ in equation (2.5). It is directly apparent from (2.5) that $s_{ZZ}(-\tau) = s_{ZZ}^*(\tau)$ (Hermitian symmetry) and $r_{ZZ}(-\tau) = r_{ZZ}(\tau)$ (symmetry). The relationship between $s_{ZZ}(\tau)$ and the spectrum $S_{ZZ}(\omega)$ is as defined in equation (2.1). The *complementary* spectrum is

$$R_{ZZ}(\omega) = \Delta \sum_{\tau=-\infty}^{\infty} r_{ZZ}(\tau) e^{-i\omega\tau\Delta},$$

where we could also define $R_{ZZ}(\omega)$ and $S_{ZZ}(\omega)$ from $\mathbb{E}\{d\Psi_Z(\omega)d\Psi_Z(-\omega)\} = R_{ZZ}(\omega) d\omega$, and $\mathbb{E}\{|d\Psi_Z(\omega)|^2\} = S_{ZZ}(\omega) d\omega$. The complementary spectrum $R_{ZZ}(\omega)$ and normal spectrum $S_{ZZ}(\omega)$ together describe the second order properties of the Fourier transform of the complex-valued process Z . We note that $R_{ZZ}(\omega)$ is *not* the relation of the orthogonal increment of Z , but rather is the Fourier transform of the relation sequence of Z . If the relation sequence, or the complementary spectrum, are zero everywhere then the process is said to be *proper*, and otherwise it is *improper* (Schreier and Scharf, 2010). We discuss the modelling implications with regards to this for complex-valued time series in Section 3.1 and also discuss tests for impropriety of time series in Section 6.2.

A key motivation behind this paper is not to interpret complex-valued time series as bivariate time series, but instead as processes that have two rotary components. This decomposes a process according

to the direction of spin. Specifically, we look at the decomposition of Z_t into two complex-valued *analytic* processes, Z^+ and Z^- , such that pointwise

$$Z_t = (Z_t^-)^* + Z_t^+ = \frac{1}{2\pi} \int_0^{\pi/\Delta} [d\Psi_Z(-\omega)e^{-i\omega t\Delta} + d\Psi_Z(\omega)e^{i\omega t\Delta}]. \quad (2.6)$$

Analytic processes such as Z^+ are best interpreted in the frequency-domain, where they have energy only at positive frequencies, and none at negative frequencies, or equivalently $Z_t^- = 0$ for all t . *Anti-analytic* processes such as Z^- are those whose conjugates are analytic processes and as such have energy only at negative frequencies, i.e. $Z_t^+ = 0$ for all t .

Equation (2.6) relates back to the decomposition we performed for real-valued processes in equation (2.4). It is natural to think of each contribution $d\Psi_Z(-\omega)e^{-i\omega t\Delta} + d\Psi_Z(\omega)e^{i\omega t\Delta}$ as mapping out a random ellipse at each frequency ω (Walden, 2013). Standard practice is therefore to describe the properties of Z via the process $\{d\Psi_Z(\omega)\}$, and to define a random ellipse at each frequency. The properties of this random ellipse is governed by how we assign the moments of $d\Psi_Z(\omega)$. The aggregation yielding Z_t from equation (2.6) will normally not map out a single ellipse in time, but rather an aggregation of ellipses, as $\text{Var}\{d\Psi_Z(\omega)\} \neq 0$ for most ω , clear from Figure 1. We already see that if $d\Psi_Z(-\omega) = d\Psi_Z^*(\omega)$ then Z_t is mapping out linear motion, whilst for any ω if exactly one of $\text{Var}\{d\Psi_Z(\pm\omega)\} = 0$ then the motion will be *circular*. Anything in between these two extremes will map out ellipses in the plane from each frequency ω . The properties of each frequency ellipse are also random, see Walden (2013), not deterministically governed by the spectral matrix. Additionally, both $s_{ZZ}(\tau)$ and $r_{ZZ}(\tau)$ map out deterministic ellipses in lag τ . Care must therefore be applied when discussing “the ellipse” of the process.

Sometimes the decomposition is made slightly differently, such that Z^+ is analytic and the second component is defined to be anti-analytic, e.g. have a spectrum only defined on negative frequencies. We prefer our representation, and consider it more natural as we then only need to specify a covariance structure between Z^+ and Z^- , as the relation sequence is zero everywhere, in contrast to Rubin-Delanchy and Walden (2008).

At first the division in equation (2.6) may seem artificial and opaque. One might argue that representing a bivariate time series as complex-valued is unnecessarily complicated, making the inclusion of *two* extra complex-valued processes seem even yet more redundant. We shall see that splitting up a process into two components in this way is natural, as it divides the process into forward rotating and reverse rotating phasors. The rotary decomposition has in fact been used as a modelling tool for many years, for example in studies of biomedical blood-flow (Olhede and Walden, 2003) and oceanographic time-series (Gonella, 1972). In particular the oceanography literature links natural phenomena with rotational spin, and as such are most naturally modelled in frequency in terms of their directionality.

Let us now be somewhat more specific in how the split into Z^+ and Z^- is done in practice, see also Olhede and Walden (2004). For a perfect split, we would need an infinitely long time sample, and so will approximate this split for any finite sample using the Discrete Fourier Transform. If we denote the Discrete Fourier Transform (defined in equation (2.2)) of finite samples from Z , Z^+ and Z^- , as $J_Z(\omega)$, $J_+(\omega)$ and $J_-(\omega)$ respectively, then

$$J_+(\omega) = \begin{cases} \frac{1}{2}J_Z(\omega), & \omega = 0, \pm\pi/\Delta, \\ J_Z(\omega), & \omega \in (0, \pi/\Delta), \\ 0, & \omega = \omega \in (-\pi/\Delta, 0), \end{cases} \quad J_-(\omega) = \begin{cases} \frac{1}{2}J_Z(\omega), & \omega = 0, \pm\pi/\Delta, \\ J_Z(-\omega), & \omega \in (0, \pi/\Delta), \\ 0, & \omega = \omega \in (-\pi/\Delta, 0) \end{cases}.$$

This yields $J_Z(\omega) = J_+(\omega) + J_-(\omega)$. We obtain Z^+ and Z^- from X and Y with $\check{Z} = \mathcal{H}Z$ denoting the discrete Hilbert transform of Z using the following operations:

$$Z^\pm = \frac{1}{2} \left(Z \pm i\check{Z} \right) = \frac{1}{2} \left\{ (X \mp \check{Y}) + i(\pm Y + \check{X}) \right\}.$$

3 Modelling techniques for complex-valued time series

When modelling complex-valued time series it is important to consider covariance between components, as these will seldom be independent, or it would not be natural to collect the series together. In this paper

we specify this relationship in the frequency-domain by modelling the *coherency* of the complex-valued time series, see also Hindberg and Hanssen (2007); Hamon and Hannan (1974). Different methods of arriving to such models are discussed in Section 3.1 and in Section 3.2. We then define an important example of such coherency models by constructing the complex-valued Matérn process in Section 3.3, which has important applications in oceanographic flow data and geophysical processes in general, as it allows for different spectral decays over different frequency ranges. In general care must be applied when modelling time series, as only specifications corresponding to valid series can be made. For example, when observing a real-valued time series we cannot make a specification not observing Hermitian symmetry in the Fourier domain. For complex-valued time series we shall see that there are no extra degrees of freedom in the frequency-domain than in the time-domain. For stationary complex-valued time series we only need to worry about modelling the Fourier transform at a frequency and its negative, as all other sets of frequencies in the spectral representation should be independent.

3.1 Cartesian coherency

A natural way to define covariance structure between the bivariate series X and Y is in the time-domain using bivariate techniques, but in this paper we do this in the frequency domain by modelling the coherency. As done in oceanography we refer to bivariate descriptions as *Cartesian*. We define the cross-spectrum between X and Y as

$$S_{XY}(\omega) = \rho_{XY}(\omega) (S_{XX}(\omega)S_{YY}(\omega))^{1/2}, \quad \rho_{XY}(\omega) = \sigma_{XY}(\omega)e^{-i\theta_{XY}(\omega)}, \quad (3.1)$$

where $\rho_{XY}(\omega)$ is the *coherency* of X and Y ; $\sigma_{XY}^2(\omega)$ is the *coherence*, and $\theta_{XY}(\omega)$ is the *group delay*, quantifying whether X or Y are leading or lagging in time at frequency-cycle ω . By necessity we constrain $0 \leq |\rho_{XY}(\omega)| \leq 1$, and $\rho_{XY}(\omega)$ is a frequency-dependent measure of coherency. We refer to $\rho_{XY}(\omega)$ as the *Cartesian coherency*. As $S_{XY}(\omega)$ is the Fourier transform of the autocovariance sequence we know that it has to exhibit Hermitian symmetry. This has the repercussion that

$$\begin{aligned} \arg\{S_{XY}(-\omega)\} &= -\{\arg S_{XY}(\omega)\}, & |S_{XY}(-\omega)| &= |S_{XY}(\omega)| \\ \Leftrightarrow \theta_{XY}(-\omega) &= -\theta_{XY}(\omega), & \sigma_{XY}(\omega) &= \sigma_{XY}(-\omega). \end{aligned} \quad (3.2)$$

Equation (3.1) is a useful representation as we can specify frequency-dependent Cartesian dependence, more convenient than the equivalent time-domain model. The model specification often becomes simpler and more interpretable. Realistic functions for $\sigma_{XY}(\omega)$ would include the logistic function

$$\sigma_{XY}(\omega) = 1 - \frac{\exp(q(\omega))}{1 + \exp(q(\omega))}, \quad q(\omega) = q_0 + q_1\omega^2 + \dots + q_r\omega^{2r}. \quad (3.3)$$

We note directly from equation (3.2) that $\sigma_{XY}(\omega)$ is an even function. This implies that we require that $q(\omega)$ is an *even* polynomial, which is exactly how this polynomial has been written down in equation (3.3). Furthermore it is reasonable to have decaying polynomials such that $\lim_{\omega \rightarrow \infty} \sigma_{XY}(\pm\omega) = 0$. This requires us to take $\lim_{\omega \rightarrow \infty} q(\omega)$ going unbounded, e.g. $q_r > 0$. The function $\theta_{XY}(\omega)$ in general takes the form

$$\theta_{XY}(\omega) = \theta_1\omega + \theta_2\omega^3 + \dots + \theta_l\omega^{2l-1}. \quad (3.4)$$

where both r and l have to be selected. The simplest choice is $r = l = 0$, which imposes a simple structure of fixed correlation across all frequencies. It may seem peculiar that a constant phase solution does not enter into equation (3.4), because we note that from equation (3.2) that $\theta_{XY}(\omega)$ is an odd function (when used over the entire frequency range). If we only look at a restricted set of frequencies, however, then Taylor expanding $\theta_{XY}(\omega)$ locally in this range means that we can obtain non-zero phase off-sets in $\theta_{XY}(\omega)$ (see Hamon and Hannan (1974, p. 137)).

It follows from equation (2.5) that the complementary spectrum of Z can be written as:

$$R_{ZZ}(\omega) = S_{XX}(\omega) - S_{YY}(\omega) + 2i\Re\{S_{XY}(\omega)\}, \quad (3.5)$$

and that $R_{ZZ}(-\omega) = R_{ZZ}(\omega)$, as both the spectral densities of real-valued processes are symmetric, as is the real part of the cross spectrum. We require $S_{XX}(\omega) = S_{YY}(\omega)$ and $\Re\{S_{XY}(\omega)\} = 0$ for the time series to be proper, i.e. for $r_{ZZ}(\tau) = 0$. This implies from equation (3.1) that to satisfy the latter condition we either require $\sigma_{XY}(\omega) = 0$ (no Cartesian coherence) or $\theta_{XY}(\omega) = \pm\pi/2$ such that X and Y are strictly “out of phase”. The latter possibility follows from the fact that a time series is zero-mean Gaussian and proper if and only if it is *circular* (i.e. a series whose properties are invariant under rotation), see Schreier and Scharf (2010). Two out-of-phase time series with the same second order properties are circular, and hence proper, for any coherence structure across frequency. An example of such would be a deterministic time series which follows an exact circle, which corresponds to $\sigma_{XY}(\omega) = 1$ and $\theta_{XY}(\omega) = \pm\pi/2$. This would lead to a purely imaginary complementary spectrum, which would not be appearing in equation (3.5).

For spatially generated processes such as the oceanographic time series we shall study subsequently, propriety is strongly tied to isotropic spatial properties, impropriety in turn implying anisotropy. Thus we can test for anisotropy in the spatial process that generates the sampled time series, and so if the complex-valued time series is generated from a spatial process, it is sensible to refer to propriety and isotropy interchangeably.

3.2 Rotary coherency

The processes Z^+ and Z^- are both complex-valued, and in general in addition to equation (3.1) we would need to describe the covariance between $d\Psi_{Z^+}(\omega)$ with $d\Psi_{Z^-}(-\omega)$, for a full description of the linear dependence between Z^+ and Z^- (Hindberg and Hanssen, 2007). As we have chosen the two to be supported only on positive frequencies however, there can be no covariance between $d\Psi_{Z^+}(\omega)$ and $d\Psi_{Z^-}(-\omega)$. Therefore in addition to the variance of $\Psi_{Z^+}(\omega)$ and $\Psi_{Z^-}(\omega)$, we only need to model their covariance at the same frequency. This is defined in the frequency-domain using the cross-spectrum for Z^+ and Z^- , which can be specified in terms of the marginal spectral densities of $S_{++}(\omega)$ and $S_{--}(\omega)$

$$S_{+-}(\omega) = \rho_{\pm}(\omega) (S_{++}(\omega)S_{--}(\omega))^{1/2}, \quad \rho_{\pm}(\omega) = \sigma_{\pm}(\omega)e^{-i\theta_{\pm}(\omega)}. \quad (3.6)$$

$0 \leq |\rho_{\pm}(\omega)| \leq 1$ specifies the coherency of Z^+ and Z^- . Equation (3.6) therefore defines frequency-dependent coherency between the positive and negative frequencies of a complex-valued time series, which we henceforth refer to as *rotary coherency*. The flexibility for $\rho_{\pm}(\omega)$ to vary across frequencies is particularly useful. In oceanographic data, for example, it is unlikely that clockwise and anti-clockwise oscillations will be correlated identically at all frequencies – but at different frequencies we would expect a different mode of correlation, see e.g. Davis et al. (1981). We can incorporate such features into this simple model. Seeing such a differentiation in real data would indicate that there are different physical scales active in the process under observation. Furthermore there is the possibility of different slopes governing the spectral decay across positive and negative frequencies. As we shall see later such would be extremely challenging to incorporate into the model for X and Y , but trivial to incorporate for the complex-valued rotary decomposition.

We can construct similar models for $\sigma_{\pm}(\omega)$ and $\theta_{\pm}(\omega)$ as proposed in equations (3.3) and (3.4), which now only need to be supported over positive frequencies (as Z^+ and Z^- are analytic). Relating correlation between negative and positive frequencies to propriety, we note that

$$\begin{aligned} r_{ZZ}(\tau) &= \mathbb{E}\{Z_t Z_{t+\tau}\} = \mathbb{E}\{[Z_t^+ + (Z_t^-)^*] [Z_{t+\tau}^+ + (Z_{t+\tau}^-)^*]\} \\ &= r_{++}(\tau) + r_{--}^*(\tau) + s_{+-}(\tau) + s_{+-}(-\tau) = s_{+-}(\tau) + s_{+-}(-\tau), \\ R_{ZZ}(\omega) &= S_{+-}(\omega) + S_{+-}(-\omega). \end{aligned}$$

We see again that $R_{ZZ}(\omega)$ is symmetric, as $R_{ZZ}(-\omega) = R_{ZZ}(\omega)$ for $\omega > 0$. Since $S_{+-}(\omega)$ is only supported over positive frequencies, for propriety we simply require that $S_{+-}(\omega) = 0$, i.e. a proper time series has no rotary coherency whatsoever, even in the case where the rotary components are out of phase (in contrast to Cartesian coherence), which is an important interpretation of propriety. We discuss how the rotary model can be used to test for temporal impropriety in Section 6.2, and again reiterate that for a stationary time series (temporal) impropriety of Z in no way equates to (spectral) impropriety of $\{d\Psi_Z(\omega)\}$. For a stationary signal, $d\Psi_{Z^+}(\omega)$ and $d\Psi_{Z^-}(\omega)$ are *always* jointly proper, even when $r_{ZZ}(\tau)$ is non-zero. Care must therefore be applied when transforming between time and frequency.

We contrast modelling in Cartesian or rotary components. It is often more natural to enforce different scaling behaviour across rotary components; especially as we may often consider the two components as independent processes. There are two arguments where we may impose different model types on the data – a separation in frequency into positively and negatively rotating components being one of them or a different structural behaviour in the Cartesian coordinates being the second. Any choice of rotation of the x/y axes might simplify the description of the signal: one would not necessarily observe the flow in the axis that has the simplest description.

Finally, to show that the model of equation (3.6) creates a valid process where the covariance/spectral matrix are both invertible (assuming $S_{++}(\omega)$ and $S_{--}(\omega)$ are themselves valid processes), we show that the spectral matrix is always nonnegative definite.

Lemma 1. *The spectral matrix given by*

$$S_{\pm}(\omega) = \begin{pmatrix} S_{++}(\omega) & S_{+-}(\omega) \\ S_{+-}^*(\omega) & S_{--}(\omega) \end{pmatrix}.$$

with $S_{+-}(\omega)$ defined in equation (3.6) is always nonnegative definite, assuming $S_{++}(\omega) \geq 0$ and $S_{--}(\omega) \geq 0$.

Proof. To complete the proof we must show that the eigenvalues are always real and nonnegative. The eigenvalues of $S_{\pm}(\omega)$ are found by solving $|S_{\pm} - \lambda I| = 0$, which yields

$$\lambda = \frac{1}{2}(S_{++} + S_{--} \pm \sqrt{(S_{++} - S_{--})^2 + 4S_{++}S_{--}|\rho_{\pm}|^2}),$$

dropping the ω notation here only for brevity. As $S_{++}(\omega) \geq 0$ and $S_{--}(\omega) \geq 0$, it follows that the eigenvalues are real. To show that both are nonnegative we make use of the fact that $|\rho_{\pm}(\omega)| \leq 1$ for all ω and hence we can say that the smallest eigenvalue

$$\lambda_{\min} \geq \frac{S_{++} + S_{--}}{2} - \frac{\sqrt{(S_{++} - S_{--})^2 + 4S_{++}S_{--}}}{2} = 0,$$

which proves all eigenvalues are nonnegative as long as $0 \leq |\rho_{\pm}(\omega)| \leq 1$. \square

Validity of dependence specification is always easier in the Fourier domain, as there are only per frequency dependencies that need to be accounted for.

3.3 The complex-valued Matérn process

The Matérn process (Gneiting et al., 2010) is a continuous stationary Gaussian process that has received much attention in the spatial and spatiotemporal modelling literature. It naturally incorporates multiscale effects. From this point, we refer to this process throughout the paper, as an important process for modelling physical phenomena. It is a representative distributional class that encapsulates many important features of stationary time series. Specifically, we refer to the Matérn process when we discuss properties of the Whittle likelihood in Section 5, provide guidelines on inference procedures in Section 6, and give simulation examples and model oceanographic flow data in Section 7.

The univariate process is defined using 3 parameters with the following covariance:

$$c_{XX}(t_1, t_2) = s_{XX}(\tau) = M(\tau; \phi, \nu, \alpha) = \frac{\phi^2 \pi^{1/2}}{2^{\nu-1} \Gamma(\nu + 1/2) \alpha^{2\nu}} (\alpha|\tau|)^{\nu} \mathcal{K}_{\nu}(\alpha|\tau|), \quad (3.7)$$

where $\tau = |t_1 - t_2|$ and $\mathcal{K}_{\nu}(\cdot)$ is the modified Bessel function of the second kind. The smoothness parameter $\nu > 0$ defines the Hausdorff dimension (equal to $\max(p, p+1-\nu)$ where p is the dimension of the process) and the differentiability of the process, the range parameter $\alpha > 0$ is a timescale parameter, where $1/\alpha$ can be referred to as the correlation length, and $\phi^2 > 0$ defines the magnitude of the variability of the process. The Matérn is a useful process in time series analysis, as the limiting behaviour over short timescales (or as $\alpha \rightarrow 0$)

is like nonstationary fractional Brownian motion, whereas the limiting behaviour over long timescales (or as $\alpha \rightarrow \infty$) is white noise – the Matérn hence provides a continuum between these two regimes over different timescales. We can therefore view the process as truly multiscale, exhibiting a well defined scaling behaviour over a range of frequencies, and then subsequently saturating to a constant energy level. The process therefore has the potential to capture complicated structure whilst simultaneously being parsimonious, yielding useful modelling potential for structured processes with which we wish to infer physically meaningful parameters from relatively few observations.

3.3.1 Multivariate Matérn process

There has been much interest in constructing valid multivariate Matérn processes in the spatial statistics literature. In particular, Gneiting et al. (2010) and Apanasovich et al. (2012) have constructed multivariate Matérn processes such that all marginal covariances and cross-covariances are themselves also of Matérn type, i.e. for dimensions i and j (where $1 \leq i, j \leq p$) of the p -dimensional process X_i

$$C_{X_i X_j}(t_1, t_2) = \rho_{ij} M(\tau; \phi_{ij}, \nu_{ij}, \alpha_{ij}),$$

where ρ_{ij} is the correlation coefficient between i and j (which is trivially set as 1 if $i = j$) and $\phi_{ij}^2 = \phi_i \phi_j$. Gneiting et al. (2010) and Apanasovich et al. (2012) proceed to specify sufficient (but not always necessary) conditions on ρ_{ij} , ν_{ij} and α_{ij} such that the covariance matrix is nonnegative definite. Gneiting et al. (2010) go further to specify necessary *and* sufficient conditions for the bivariate Matérn process ($p = 2$) to have cross-covariances that are of Matérn type and for the covariance matrix to be nonnegative definite, which we provide as part of Appendix A. In this paper, however, we choose to specify the cross-covariance structure in the frequency-domain. Our rationale for this choice is twofold. First, for the oceanography application we study, it is easier to specify the covariance of the flow process in terms of specially chosen complex-valued processes from physical considerations. Second, it is very easy to check whether a specified choice corresponds to a valid covariance (as in Lemma 1), unlike the torturous calculations sometimes necessary in the time domain.

The spectrum of the sampled Matérn has a succinct and interpretable representation:

$$S_{XX}(\omega) = \sum_{k=-\infty}^{\infty} \frac{\phi^2}{((\omega + 2\pi k)^2 + \alpha^2)^{\nu+1/2}}, \quad (3.8)$$

where the summation over intervals of 2π is required to fold in aliased frequencies such that the spectrum is of the sampled and not continuous process. We can specify that each of Z^+ , Z^- , X and Y are Matérn processes with spectra given by equation (3.8) and covariance given by equation (3.7). We now denote parameters of each process by ϕ_X , ϕ_+ and so on, which are permitted to differ between the processes. If we specify cross-spectra as in equation (3.1) or (3.6) then it is automatic from Lemma 1 that the overall bivariate process is valid. By “valid” we mean it possesses an invertible covariance/spectral matrix, but not necessarily a cross-covariance/cross-spectrum that is also Matérn, *unlike* the case of Gneiting et al. (2010) and Apanasovich et al. (2012). For the latter to be the case, we require that $\alpha_X = \alpha_Y$ (or $\alpha_+ = \alpha_-$ for complex-valued processes) and that $\rho(\omega)$ is real-valued and constant across frequency, but ν and ϕ can vary between components³. This specification is in this sense less general than Gneiting et al. (2010), as they allow instances where $\alpha_X \neq \alpha_Y$ in their bivariate Matérn definition. Although we note that our construction allows cross-covariances that are not of Matérn type but still specify a valid bivariate distribution. Moreover, we can construct components that have frequency-dependent coherence, as $\rho(\omega)$ is permitted to vary across frequency, whereas Gneiting et al. (2010) only permit a constant correlation structure across time-lag and hence frequency. We verify that the case $\alpha_X = \alpha_Y$ (and also $\alpha_+ = \alpha_-$ for complex-valued processes) is a valid bivariate Matérn, as per the definition of Gneiting et al. (2010), for constant $0 \leq |\rho_{XY}(\omega)| \leq 1$ in Appendix A.

³One could of course have $\alpha_+ \neq \alpha_-$ or $\alpha_X \neq \alpha_Y$ and then construct $\rho(\omega)$ to vary across frequencies in such a way that the resulting cross-spectrum is still a Matérn, but this is artificial in the context of applications and not considered here.

3.3.2 Parametric rotary models

Finally, it is interesting to discuss the Matérn family in somewhat more of a framework for the types of analyses that will be appropriate for the motivating data example in Section 7, which examines oceanographic flow processes. We define the deformation operator $\mathcal{D}_{r,\beta}Z_t^+ = rZ_{\beta t}^+$, and take $Z_t^+ = \mathcal{D}_{r,\beta}U_t$, $Z_t^- = \mathcal{D}_{q,\beta}U_t + \mathcal{D}_{u,\gamma}V_t$, where we assume that U_t and V_t are independent, but also correspond to some stochastic processes with the same parameters. This deforms the basic flow processes, and introduces new forms of correlations. It follows that $\text{Cov}\{Z_t^+, Z_{t+\tau}^-\} = rqc_{UU}(\beta t, \beta t + \beta\tau) = rqs_{UU}(\beta\tau)$, and we see that the processes remain jointly stationary. The basic scale of variation has changed to take account of the scaling of β . If we look at the cross-spectrum then it transpires that it takes the form

$$S_{+-}(\omega) = \int s_{+-}(\tau)e^{-i\omega\tau} d\tau = \int rqs_{++}(\beta\tau) e^{-i\omega\tau} d\tau = rq\frac{1}{\beta}S_{++}\left(\frac{\omega}{\beta}\right).$$

We therefore find that if $S_{++}(\omega)$ takes the Matérn form, then so does $S_{+-}(\omega)$ except with altered parameters. Both α and ϕ change from such deformations but not ν .

Starting with the rotary components, the most general form of spectral matrix we shall posit is given by

$$S_{\pm}(\omega) = \begin{pmatrix} \frac{\phi_+^2}{(\omega^2 + \alpha_+^2)^{\nu_+ + 1/2}} & \frac{\rho_{\pm}(\omega)\phi_+\phi_-}{(\omega^2 + \alpha_+^2)^{\nu_+ / 2 + 1/4}(\omega^2 + \alpha_-^2)^{\nu_- / 2 + 1/4}} \\ \frac{\rho_{\pm}^*(\omega)\phi_+\phi_-}{(\omega^2 + \alpha_+^2)^{\nu_+ / 2 + 1/4}(\omega^2 + \alpha_-^2)^{\nu_- / 2 + 1/4}} & \frac{\phi_-^2}{(\omega^2 + \alpha_-^2)^{\nu_- + 1/2}} \end{pmatrix}.$$

This matrix allows for a different smoothness in the Z^+ and Z^- processes. One example of how such behaviour could arise would be if there were basic rescalings of the same types of processes, as discussed above. This type of model leads to a spectral matrix of

$$S_{\pm}(\omega) = \frac{1}{(\omega^2 + \alpha^2)^{\nu + 1/2}} \begin{pmatrix} \phi_+^2 & \rho_{\pm}(\omega)\phi_+\phi_- \\ \rho_{\pm}^*(\omega)\phi_+\phi_- & \phi_-^2 \end{pmatrix}. \quad (3.9)$$

This type of bivariate model would regulate *the same* scaling behaviour between Z^+ and Z^- , but the energy of each process being individually regulated by ϕ_+^2 and ϕ_-^2 . The correlation has two aspects: a magnitude of $\sigma_{\pm}(\omega)$ and a group delay of $\theta_{\pm}(\omega)$ (from equation (3.6)). We use the model of equation (3.9) to capture both isotropic and anisotropic structure in oceanographic flow processes in Section 7.2.

The usefulness of the Matérn family is that multiscale behaviour is achievable from one single family. The more subtle issue however is the relationship between the rotary and Cartesian decompositions. Specifying a Matérn process in one decomposition will, in general, force the other to possess a mixture of Matérns. A Matérn specified in Z^+ and Z^- only specifies a single Matérn in X and Y if $\alpha_+ = \alpha_-$, $\nu_+ = \nu_-$ and $\sigma_{\pm}(\omega)$ and $\theta_{\pm}(\omega)$ are constant across frequencies⁴ (and similarly in the opposite direction). Although we note that in such cases the cross-spectra $S_{XY}(\omega)$ and $S_{+-}(\omega)$ are in general complex-valued and out-of-phase. This means that a simple model in one decomposition does not lead to a simple model in the other, and the practitioner must therefore understand the data and the processes driving the data to find the simplest decomposition in which to model.

4 The Whittle Likelihood

Theoretically it is possible to implement standard maximum likelihood estimation in the time domain, see Dahlhaus (1988). We choose not to implement this strategy for two reasons. First, it is computationally very expensive to invert full time domain covariance matrices (as we shall see in Section 7). Second, we wish to be able to parameterise the structure in terms of properties of Z^+ and Z^- , which is not conveniently implemented in the time-domain, as discussed in Section 3.1. The method we shall choose, however, will

⁴Unless we of course construct unrealistic tailored forms for $\sigma_{\pm}(\omega)$ and $\theta_{\pm}(\omega)$ such that the cross-spectra are coincidentally of Matérn form even when $\alpha_{\pm} \neq \alpha_{\pm}$ and/or $\nu_{\pm} \neq \nu_{\pm}$.

approximate the time-domain log-likelihood, so to be able to compare the properties of estimators we shall also give the form of the time-domain function. In the case of a zero-mean real-valued process X the log-likelihood can be written as

$$\ell_t(\boldsymbol{\theta}) = -\frac{1}{2} \log |C_X(\boldsymbol{\theta})| - \frac{1}{2} X^T C_X^{-1}(\boldsymbol{\theta}) X, \quad C_X(\boldsymbol{\theta}) = \mathbb{E}(X X^T). \quad (4.1)$$

To find the log-likelihood for the bivariate process linking X and Y we concatenate the two time domain samples into a single vector: $U^T = (X^T \ Y^T)$. We write the covariance matrix of this vector as $C_U(\boldsymbol{\theta}) = \mathbb{E}(U U^T)$. The log-likelihood of the vector U can be written as

$$\ell_t(\boldsymbol{\theta}) = -\frac{1}{2} \log |C_U(\boldsymbol{\theta})| - \frac{1}{2} U^T C_U^{-1}(\boldsymbol{\theta}) U, \quad (4.2)$$

in direct parallel with equation (4.1). The data is observed in the time-domain, and so using the maximum likelihood principle, inferences should be based on equations (4.1) and (4.2) to achieve good properties of any estimator. Thus we would like to form

$$\widehat{\boldsymbol{\theta}}^{(t)} = \arg \max_{\boldsymbol{\theta} \in \Theta} \ell_t(\boldsymbol{\theta}).$$

Any other estimator will be compared with the properties of this quantity, which is computationally expensive to obtain.

A standard technique to approximating equation (4.1) is in the frequency domain, from the seminal work of Whittle (1953b). This is inevitably strongly linked with approximating $C_X(\boldsymbol{\theta})$ using a Fourier representation, and rests on properties of Toeplitz matrices. For a single real-valued time series the Whittle likelihood is given by

$$\ell_W(\boldsymbol{\theta}) = - \sum_{\omega \in \Omega} [\log \{S_{XX}(\omega; \boldsymbol{\theta})\} + J_X^H(\omega) S_{XX}^{-1}(\omega; \boldsymbol{\theta}) J_X(\omega)], \quad (4.3)$$

where $\Omega \subset [0, \frac{\pi}{\Delta}]$. If Ω is substantially smaller in its range than the full range of frequencies then the Whittle likelihood can be considered as a semi-parametric fitting procedure (see Section 6.1 for more discussion), where we only specify a parametric model of $S(\omega)$ for $\omega \in \Omega$. The Whittle likelihood *approximates* the time-domain likelihood, i.e. $\ell_t(\boldsymbol{\theta}) \approx \ell_W(\boldsymbol{\theta})$, and this statement can be made precise (Dzhaparidze and Yaglom, 1983).

4.1 The Blurred Whittle Likelihood

The Whittle likelihood is *not* equivalent to the likelihood for the discrete Fourier transform $\{J_X(\omega)\}$. This is because the absolute square of the discrete Fourier transform (the periodogram) is not in general an unbiased measure of the true spectrum for finite sample sizes, due to the blurring caused by leakage and additional aliasing effects. Under fairly general assumptions, however, the distribution of the Fourier transform evaluated at Fourier frequencies is jointly Gaussian. We therefore define an alternative likelihood function to $\ell_W(\boldsymbol{\theta})$ and $\ell_t(\boldsymbol{\theta})$ based on $J_X = (J_X(\omega_0), \dots, J_X(\omega_{\max}))$, written as

$$\begin{aligned} \ell_f(\boldsymbol{\theta}) &= - \sum_{\omega \in \Omega} \left[\log \{ \overline{S}_{XX; \boldsymbol{\theta}}(\omega) \} + J_X^H(\omega) \overline{S}_{XX; \boldsymbol{\theta}}^{-1}(\omega) J_X(\omega) \right], \\ \overline{S}_{XX}(\omega; \boldsymbol{\theta}) &= \int_{-\pi/\Delta}^{\pi/\Delta} S_{XX}(\omega'; \boldsymbol{\theta}) \mathcal{F}_{N, \Delta}(\omega' - \omega) d\omega', \quad \mathcal{F}_{N, \Delta}(\omega) = \frac{\Delta}{2\pi N} \frac{\sin^2(N\omega\Delta/2)}{\sin^2(\omega\Delta/2)}. \end{aligned} \quad (4.4)$$

$\mathcal{F}_{N, \Delta}(\omega)$ corresponds to the Fejér kernel. The variance of the discrete Fourier transform now experiences finite sampling effects and the bias in the estimation caused by leakage and aliasing has been removed. This is because we have replaced $S_{XX}(\omega)$ by $\overline{S}_{XX}(\omega)$. We call this the *blurred Whittle likelihood* and document its performance in a Monte Carlo study in Section 7.1. The usual form of the Whittle likelihood

can be computed efficiently by using the fast Fourier transform to calculate the DFT, which is an $\mathcal{O}(N \log N)$ operation. The blurred Whittle likelihood however, is a little more complicated to compute as $\bar{S}_{XX}(\omega)$ must now be calculated. The best way to do this is actually from the time-domain by Fourier transforming the expected biased sample autocovariance

$$\begin{aligned} \bar{S}_{XX}(\omega; \boldsymbol{\theta}) &= \Delta \sum_{\tau=-(N-1)}^{N-1} \mathbb{E}(\hat{s}_{XX}(\tau)) e^{-i\omega\tau\Delta} \\ &= 2\Delta \sum_{\tau=0}^{N-1} \left(1 - \frac{\tau}{N}\right) \Re\{s_{XX}(\tau; \boldsymbol{\theta})\} e^{-i\omega\tau\Delta} - \Delta \Re\{s_{XX}(0; \boldsymbol{\theta})\}. \end{aligned} \quad (4.5)$$

This equation makes use of the fact that the periodogram forms a Fourier pair with the biased sample autocovariance sequence, $\{\hat{s}_{XX}(\tau)\}$. The bias has the effect of multiplying the autocovariance sequence with the triangle kernel. This can also be computed in $\mathcal{O}(N \log N)$ operations. This makes this form of likelihood very efficient to compute. In fact, the aliasing effects are already taken account of in equation (4.5), whereas $\ell_W(\boldsymbol{\theta})$ requires the approximation of an infinite summation (see equation (3.8) for example) in the likelihood, so the blurred form of the likelihood can in fact be more efficient to compute, as we shall see in Section 7.1. This effect is especially pronounced for the types of data we consider. If the closed form of the autocovariance sequence is not known, then we can inverse Fourier transform the spectrum of the continuous time process to find the exact autocovariance sequence numerically. Subsequently we would take the Fourier transform multiplied with the triangle kernel (or the equivalent kernel for tapered estimates) to recover an exact estimate of $\bar{S}_{XX}(\omega)$, still in $\mathcal{O}(N \log N)$ operations.

In general even the independence between frequencies implicit in equation (4.4) is not necessarily appropriate for finite samples. This correlation exists because even if the Fejér kernel decays, this decay is not necessarily sufficiently rapid. A possibility would therefore be to account for the correlation between frequencies closely spaced to one another. The objective function in equation (4.4) would be adjusted to account for the correlation between all Fourier frequencies. This correlation is present in *all* finite sample sizes unless $S_{XX}(\omega)$ is exactly constant. We could therefore define a fourth objective function $\ell_{fc}(\boldsymbol{\theta})$ that takes account of this finite sample correlation. This would not be computationally efficient to evaluate, and we will see in Section 5 that in any case it is reasonable to ignore these correlations in the likelihood, particularly for the key physical processes that we focus on.

4.2 Parametric Tapered Whittle Inference

There is also a fifth possible likelihood that could be defined by extending the Whittle likelihood to tapered discrete Fourier transforms, e.g. Thomson (1990). This corresponds to replacing the direct spectral estimator of $J_X(\omega)$ in equation (2.2) using the taper $\{h_t\}$

$$J_X(\omega; h) = \Delta^{1/2} \sum_{t=1}^N h_t X_t e^{-i\omega t\Delta}, \quad \sum_{t=1}^N h_t^2 = 1,$$

where h_t is real-valued. The tapered Fourier transform is used to reduce bias in non-parametric estimation from leakage (Percival and Walden, 1993). In the parametric setting we take

$$\ell_h(\boldsymbol{\theta}) = - \sum_{\omega \in \Omega} [\log \{S_{XX}(\omega; \boldsymbol{\theta})\} + J_X^H(\omega; h) S_{XX}^{-1}(\omega; \boldsymbol{\theta}) J_X(\omega; h)]. \quad (4.6)$$

Setting $h_t = 1/\sqrt{N}$ recovers the periodogram estimate of equation (4.3). Velasco and Robinson (2000) demonstrated that for certain discrete processes it is beneficial to use this estimator, ahead of $\ell_W(\boldsymbol{\theta})$, for parameter estimation – particularly when a suitable taper is used and the parameters controlling the spectral decay of processes are high. Whilst this is true, tapering will *not* remove all leakage effects, and the issue of

aliasing for continuous sampled process remains. We therefore define a final sixth possible type of likelihood, which accounts for finite sampling effects from tapering:

$$\begin{aligned} \ell_{hf}(\boldsymbol{\theta}) &= - \sum_{\omega \in \Omega} \left[\log \{ \bar{S}_{XX}(\omega; h, \boldsymbol{\theta}) \} + J_X^H(\omega; h) \bar{S}_{XX}^{-1}(\omega; h, \boldsymbol{\theta}) J_X(\omega; h) \right], \\ \bar{S}_{XX}(\omega; h, \boldsymbol{\theta}) &= \int_{-\pi/\Delta}^{\pi/\Delta} S_{XX}(\omega'; \boldsymbol{\theta}) \mathcal{H}_{N,\Delta}(\omega' - \omega) d\omega', \quad \mathcal{H}_{N,\Delta}(\omega) = \Delta \left| \sum_{t=1}^N h_t e^{-i\omega t \Delta} \right|^2. \end{aligned} \quad (4.7)$$

We call this the *tapered blurred Whittle likelihood*, and can be computed using a similar $\mathcal{O}(N \log N)$ calculation to equation (4.5) to find $\bar{S}_{XX}(\omega; h)$:

$$\bar{S}_{XX}(\omega; h, \boldsymbol{\theta}) = 2\Delta \sum_{\tau=0}^{N-1} \left(\Re \{ s_{XX}(\tau; \boldsymbol{\theta}) \} \sum_{t=1}^{N-\tau} h_t h_{t+\tau} \right) e^{-i\omega \tau \Delta} - \Delta \Re \{ s_{XX}(0; \boldsymbol{\theta}) \}.$$

The kernel $\sum_{t=1}^{N-\tau} h_t h_{t+\tau}$ must be pre-computed (unless it has an analytic form) which requires $\mathcal{O}(N^2)$ operations but can be stored for each taper and data-length N and does not have to be recomputed each time when performing numerical optimisation.

The practitioner is therefore free to select between a tapered or periodogram spectral estimate in the same way as before, but can now account for finite sample bias effects by using our proposed methods. The tradeoff lies in the fact that tapering increases local bias and correlations between local frequencies, but the periodogram may exhibit greater global bias and correlation with other frequencies; this depends on the degree of dynamic range of the observed process in frequency. We explore these ideas further and demonstrate the importance of blurring the likelihood through Monte Carlo simulations in Section 7.1.

4.3 The Whittle Likelihood for Complex-Valued Time Series

In this section we construct the Whittle Likelihood for complex-valued time series, taking into account the points raised in Section 4.1. We construct likelihoods for both decompositions (Cartesian and rotary) specified in Section 2.2, where we can then use corresponding parametric models for the coherency specified in Sections 3.1 and 3.2. The Cartesian decomposition in fact follows directly from the bivariate Whittle likelihood, see also Whittle (1953a). Specifically, we define the spectral matrix as

$$S_U(\omega) = \begin{pmatrix} S_{XX}(\omega) & S_{XY}(\omega) \\ S_{XY}^*(\omega) & S_{YY}(\omega) \end{pmatrix}.$$

Note that this is a natural parameterisation of bivariate spectral properties, see Wahba (1971). Linked with the spectral matrix is the Fourier transform of $\{X_t\}$ and $\{Y_t\}$, naturally concatenated at a given frequency ω to a single vector which we denote as

$$J_U(\omega) = \begin{pmatrix} J_X(\omega) \\ J_Y(\omega) \end{pmatrix} = \left(\frac{\Delta}{N} \right)^{1/2} \sum_{t=1}^N \begin{pmatrix} X_t \\ Y_t \end{pmatrix} e^{-i\omega t \Delta}.$$

Using this parameterisation it follows that the bivariate likelihood is (Whittle, 1953a)

$$\ell_W(\boldsymbol{\theta}) = - \sum_{\omega \in \Omega} \left[\log \{ \det (S_U(\omega; \boldsymbol{\theta})) \} + J_U^H(\omega) S_U^{-1}(\omega; \boldsymbol{\theta}) J_U(\omega) \right]. \quad (4.8)$$

We note that this likelihood is the bivariate form of equation (4.3), and it approximates the bivariate likelihood of $\ell_t(\boldsymbol{\theta})$ given in equation (4.2). Integrally related to forming a likelihood is specifying a distribution for a data sample, and this is complicated when the data is complex-valued. We would like to note that considerable efforts have been spent clarifying the distribution of a complex-valued quantity; in parts correcting the common misconception on the freedom of freely specifying a density both to Z and Z^* . The

most satisfying approach is to write down the density in terms of the real-valued observables, and then algebraically reformulate this as a function of Z and Z^* (Olhede, 2006), permitting us to still formulate models conveniently for the complex-valued signal directly.

To reformulate (4.8) in terms of the rotary decomposition we start by defining

$$J_{\pm}(\omega) = \begin{pmatrix} J_+(\omega) \\ J_-(\omega) \end{pmatrix} = \left(\frac{\Delta}{N}\right)^{1/2} \sum_{t=1}^N \begin{pmatrix} Z_t^+ \\ Z_t^- \end{pmatrix} e^{-i\omega t \Delta},$$

as the discrete Fourier transform of the rotary components. We wish to rewrite the Fourier transform of Z^+ and Z^- in terms of the Fourier transforms of X and Y . We define the 2π periodic sign function to be $\Xi(\omega)$. Therefore we have that $J_{\check{X}}(\omega) = -i\Xi(\omega)J_X(\omega)$, where $\check{X} = \mathcal{H}X$ is the Discrete Hilbert Transform of X and similarly for Y (as discussed in Section 2.2). It therefore follows from equation (2.2) that there is a simple linear relationship between $J_{\pm}(\omega)$ and $J_U(\omega)$

$$J_{\pm}(\omega) = \begin{pmatrix} J_+(\omega) \\ J_-(\omega) \end{pmatrix} = \frac{1 + \Xi(\omega)}{2} \begin{pmatrix} 1 & i \\ 1 & -i \end{pmatrix} J_U(\omega), \quad J_U(\omega) = \frac{1}{2} \begin{pmatrix} 1 & 1 \\ -i & i \end{pmatrix} J_{\pm}(\omega) \quad \omega > 0,$$

and $\mathbf{0}$ otherwise. We can now rewrite the Whittle likelihood using this decomposition. We start from equation (4.8) and take only positive frequencies in Ω . Then

$$\begin{aligned} \ell_W(\boldsymbol{\theta}) &= - \sum_{\omega \in \Omega} [\log \{\det(S_U(\omega; \boldsymbol{\theta}))\} + J_U^H(\omega) S_U^{-1}(\omega; \boldsymbol{\theta}) J_U(\omega)] \\ &\stackrel{C}{=} - \sum_{\omega \in \Omega} [\log \{\det(S_{\pm}(\omega; \boldsymbol{\theta}))\} + J_{\pm}^H(\omega) S_{\pm}^{-1}(\omega; \boldsymbol{\theta}) J_{\pm}(\omega)], \end{aligned} \quad (4.9)$$

where $\stackrel{C}{=}$ denotes equality up to an additive constant. We have defined the rotary spectral matrix as, for a given $\boldsymbol{\theta}$,

$$\begin{aligned} S_{\pm}^{-1}(\omega) &= \frac{1}{4} \begin{pmatrix} 1 & i \\ 1 & -i \end{pmatrix} S_U^{-1}(\omega) \begin{pmatrix} 1 & 1 \\ -i & i \end{pmatrix} \\ &= \frac{1}{4\det(S_U(\omega))} \begin{pmatrix} 1 & i \\ 1 & -i \end{pmatrix} \begin{pmatrix} S_{YY}(\omega) & -S_{XY}(\omega) \\ -S_{XY}^*(\omega) & S_{XX}(\omega) \end{pmatrix} \begin{pmatrix} 1 & 1 \\ -i & i \end{pmatrix}. \end{aligned} \quad (4.10)$$

By inverting equation (4.10) we find that

$$\begin{aligned} S_{\pm}(\omega) &= \begin{pmatrix} S_{XX}(\omega) + S_{YY}(\omega) + 2\Im\{S_{XY}(\omega)\} & S_{XX}(\omega) - S_{YY}(\omega) + 2i\Re\{S_{XY}(\omega)\} \\ S_{XX}(\omega) - S_{YY}(\omega) - 2i\Re\{S_{XY}(\omega)\} & S_{XX}(\omega) + S_{YY}(\omega) - 2\Im\{S_{XY}(\omega)\} \end{pmatrix} \\ &= \begin{pmatrix} S_{++}(\omega) & S_{+-}(\omega) \\ S_{+-}^*(\omega) & S_{--}(\omega) \end{pmatrix}. \end{aligned} \quad (4.11)$$

which follows directly from equation (4.9), and using that $\det(S_{\pm}(\omega)) = 4\det(S_{XY}(\omega))$.

We therefore have two parameterisations of one *single* likelihood, *i.e.* equations (4.8) and (4.9), and define the complex-valued Whittle likelihood for rotary components in equation (4.9), with $S_{\pm}(\omega)$ given in equation (4.11). Note that it is identical in form to the bivariate likelihood given in equation (4.8). The likelihoods sum to the same quantity, or at least up to an additive constant. The key difference however is that we specify rotary spectra in $S_{\pm}(\omega)$ rather than Cartesian spectra in $S_U(\omega)$. The rotary spectra can be written in terms of the Cartesian components X and Y (from equation (4.11)), for a given $\boldsymbol{\theta}$,

$$S_U(\omega) = \frac{1}{4} \begin{pmatrix} S_{++}(\omega) + S_{--}(\omega) + 2\Re\{S_{+-}(\omega)\} & 2\Im\{S_{+-}(\omega)\} + i(S_{++}(\omega) - S_{--}(\omega)) \\ 2\Im\{S_{+-}(\omega)\} - i(S_{++}(\omega) - S_{--}(\omega)) & S_{++}(\omega) + S_{--}(\omega) - 2\Re\{S_{+-}(\omega)\} \end{pmatrix}.$$

Thus if the spectral matrix is defined in Z^+ and Z^- , then the spectral matrix in X and Y will not be in an easily interpretable form. For example, if the cross-spectrum between two different analytic processes

Z^+ and Z^- is real-valued then the cross-spectrum of X and Y will be necessarily imaginary – meaning the Cartesian coherence is out of phase. In addition, if Z^+ and Z^- exhibit different decaying spectral slopes, then the process will be “multifractal” in X and Y . If we wish to retain the blurred likelihood then we find that

$$\begin{aligned}\ell_f(\boldsymbol{\theta}) &= -\sum_{\omega \in \Omega} \left[\log \{ \det (\bar{S}_{\pm}(\omega; \boldsymbol{\theta})) \} + J_{\pm}^H(\omega) \bar{S}_{\pm}^{-1}(\omega; \boldsymbol{\theta}) J_{\pm}(\omega) \right], \\ \bar{S}_{\pm}(\omega; \boldsymbol{\theta}) &= \int_{-\pi/\Delta}^{\pi/\Delta} S_{\pm}(\omega'; \boldsymbol{\theta}) \mathcal{F}_N(\omega' - \omega) d\omega',\end{aligned}\tag{4.12}$$

and similarly for tapered versions. We can compute the likelihood in the same way for Cartesian components (by replacing S_U with \bar{S}_U in Equation (4.8)). The same approaches as discussed in Sections 4.1 and 4.2 can be used to compute the blurred likelihood, as we perform later in Section 7.2.

Finally, one of the clear advantages of using either of equation (4.9) or (4.12) is that we have clearly decoupled into negative and positive frequencies. If the special case of no off-diagonal entries in $S_{\pm}(\omega)$ holds (i.e. the process is proper) then we can separate inferences for $S_{++}(\omega)$ and $S_{--}(\omega)$, unless there are parameters used in both the specification of $S_{++}(\omega)$ and $S_{--}(\omega)$. This is because the likelihood will factorise into independent contributions, and so they will be independent contributions to the sum of the log-likelihood. In this scenario the set of periodogram values at positive frequencies will be sufficient statistics for the parameters of the positive frequencies, and the set of periodogram values at negative frequencies will be sufficient statistics for the parameters of the negative frequencies.

5 Properties of Whittle Estimators

We shall establish some basic properties of Whittle estimators, and argue why blurring is important for reducing bias, as well as deliver reasonable large but finite sampling properties of the estimators. We shall consider this discussion for scalar parameters, this is in order to derive simplifications in the discussion. In general most of our observations are valid for vector-valued parameters, and indeed there are then complications where the high or low value of one parameter may strongly influence the estimation of other parameters. The basic properties of a given Whittle estimator mainly follows from the score equation, namely

$$\frac{d\ell_W(\theta)}{d\theta} = -\sum_{\omega \in \Omega} Y(\omega; \theta), \quad Y(\omega; \theta) = \frac{d \log \{|S_U(\omega; \theta)|\}}{d\theta} + J_U^H(\omega) \frac{d}{d\theta} S_U^{-1}(\omega; \theta) J_U(\omega).$$

The Whittle estimator is determined by solving $\frac{d\ell_W(\hat{\theta})}{d\theta} = 0$. We are interested in the performance of estimators given $\bar{S}_U(\omega; \theta) = \mathbb{E}(|J_U(\omega)|^2) \neq S_U(\omega)$. We first give a form for the expectation of this random variable.

Proposition 1. *The expectation of the periodogram takes the form*

$$\bar{S}_U(\omega; \theta) = S_U(\omega; \theta) + \frac{1}{2} \tilde{S}_U(\theta) \alpha_N^2(\omega) + \max_{\omega' \notin (\omega - \frac{b}{\sqrt{N}}, \omega + \frac{b}{\sqrt{N}})} S_U(\omega'; \theta) \mathcal{O}\left(\frac{1}{N^{1/2}}\right),$$

where $\alpha_N^2(\omega) = 1/(6N)$ and $|\tilde{S}_U(\theta)| \leq \max_{\omega' \in [\omega - \frac{c}{\sqrt{N}}, \omega + \frac{c}{\sqrt{N}}]} S_U^{(2)}(\omega'; \theta)$.

Proof. For simplicity take $\Delta = 1$. We can then separate the expectation in terms of narrow-band and

broad-band bias, see (Bloomfield, 2004),

$$\begin{aligned}
\bar{S}_U(\omega; \theta) &= \int_{-\pi}^{\pi} S_U(\omega'; \theta) \mathcal{F}_N(\omega' - \omega) d\omega' \\
&= \int_{\omega - \frac{b}{\sqrt{N}}}^{\omega + \frac{b}{\sqrt{N}}} \left[S_U(\omega; \theta) + \frac{1}{2} S_U^{(2)}(\omega''; \theta) (\omega' - \omega)^2 \right] \mathcal{F}_N(\omega' - \omega) d\omega' \\
&\quad + \int_{\omega' \notin \left(\omega - \frac{b}{\sqrt{N}}, \omega + \frac{b}{\sqrt{N}}\right)} S_U(\omega'; \theta) \mathcal{F}_N(\omega' - \omega) d\omega' \\
&= S_U(\omega; \theta) + R_N^{(1)}(\theta) + R_N^{(2)}(\theta).
\end{aligned}$$

We see that the narrow-band bias $R_N^{(1)}(\theta)$ is going to be dominated by

$$|R_N^{(1)}(\theta)| \leq \frac{1}{2} \int_{\omega - \frac{b}{\sqrt{N}}}^{\omega + \frac{b}{\sqrt{N}}} |S_U^{(2)}(\omega''; \theta)| (\omega' - \omega)^2 \mathcal{F}_N(\omega' - \omega) d\omega' \sim \frac{1}{2} S_U^{(2)}(\omega; \theta) \alpha_N^2 (1 + o(1)),$$

where $\alpha_N^2 = \int_{-\pi}^{\pi} (\omega' - \omega)^2 \mathcal{F}_N(\omega' - \omega) d\omega'$ and $\alpha_N^2 = \frac{1}{6N}$. In contrast it follows that the broad-band bias $R_N^{(2)}(\theta)$ is simply

$$\begin{aligned}
R_N^{(2)}(\theta) &= \int_{\omega' \notin \left(\omega - \frac{b}{\sqrt{N}}, \omega + \frac{b}{\sqrt{N}}\right)} S_U(\omega'; \theta) \mathcal{F}_N(\omega' - \omega) d\omega' \\
&\leq \max_{\omega' \notin \left(\omega - \frac{b}{\sqrt{N}}, \omega + \frac{b}{\sqrt{N}}\right)} S_U(\omega'; \theta) \int_{bN^{1/2}}^{\pi N} \frac{2 \sin^2(\nu)}{2\pi\nu^2} d\nu.
\end{aligned}$$

Note that $\int_{bN^{1/2}}^{\pi N} \frac{2 \sin^2(\nu)}{2\pi\nu^2} d\nu = \mathcal{O}\left(\frac{1}{N^{1/2}}\right)$, and is clearly decaying.

Thus $R_N^{(2)}(\theta) = \max_{\omega' \notin \left(\omega - \frac{b}{\sqrt{N}}, \omega + \frac{b}{\sqrt{N}}\right)} S_U(\omega'; \theta) \mathcal{O}\left(\frac{1}{N^{1/2}}\right)$. \square

If we are trying to estimate very large and variable contributions to the spectrum such as peaks, then the narrow-band bias matters more. If on the other hand we are trying to estimate regions of the spectrum with little variation and there are peaks elsewhere, then broadband bias becomes more significant. From Proposition 1 we therefore have

$$\mathbb{E} \left\{ \frac{d\ell_W(\theta_0)}{d\theta} \right\} = - \sum_{\omega \in \Omega} \mathbb{E}(Y(\omega; \theta_0)) = \sum_{\omega \in \Omega} \left[\frac{\frac{d}{d\theta} S_U(\omega; \theta_0)}{S_U(\omega; \theta_0)} \left(\frac{R_N^{(1)}(\theta_0)}{S_U(\omega; \theta_0)} + \frac{R_N^{(2)}(\theta_0)}{S_U(\omega; \theta_0)} \right) \right].$$

In a typical model such as a peaked spectrum with a given location (e.g. $S_U(\omega) \propto |\omega - \omega_o|^{-2\beta}$, and an infinite peak at that location we would assume that $R_N^{(1)}(\theta)$ dominates: this will however only effect a range of frequencies, the remaining $\mathcal{O}(N)$ frequencies will be mainly affected by broad-band bias, namely $R_N^{(2)}(\theta)$. Thus *unless* we are at values where the spectrum is highly dynamic (near the peak), the broad-band bias is going to have a stronger impact. These issues are avoided using the blurred likelihood as then $\mathbb{E} \left\{ \frac{d\ell_f(\theta_0)}{d\theta} \right\} = 0$.

Now the second quantity we shall need in order to understand the score is the covariance of the periodogram across different frequencies. We note that for a Gaussian time series the covariance of the DFT is

$$\text{Cov} \left\{ \hat{S}_U(\omega_1; \theta), \hat{S}_U(\omega_2; \theta) \right\} = |\mathbb{E}\{J(\omega_1)J^*(\omega_2)\}|^2,$$

which has the implication that the correlation can only be positive. We shall assume a form of

$$|\mathbb{E}\{J(\omega_j)J^*(\omega_k)\}| \leq h \frac{\sqrt{S(\omega_j)S(\omega_k)}}{|j - k|^\gamma}, \quad j - k \neq 0,$$

that is, decaying correlation, depending on the distance between frequencies. With this assumption we then have that the off-diagonal entries accumulate moderately

$$\left| \sum_{\omega_2 \neq \omega_1 \in \Omega} \sum_{\omega_1 \in \Omega} \text{Cov}\{Y(\omega_1; \theta), Y(\omega_2; \theta)\} \right| \leq \frac{2N^2}{N^{2(1+\gamma)}} \sum_{j>k} S'(\omega_1)S'(\omega_2) \frac{h^2 N^{2\gamma}}{|j-k|^{2\gamma}} = \mathcal{O}(N^{2-2\gamma}).$$

We also calculate the diagonal aggregation, which is

$$\begin{aligned} \sum_{\omega_1 \in \Omega} \text{Var}\{Y(\omega_1; \theta)\} &= \sum_{\omega_1 \in \Omega} \frac{[S'(\omega_1)]^2}{S^4(\omega_1)} \bar{S}_U^2(\omega; \theta) \\ &= \sum_{\omega_1 \in \Omega} \frac{[S'(\omega_1)]^2}{S^4(\omega_1)} \left[S_U(\omega; \theta) + R_N^{(1)}(\theta) + R_N^{(2)}(\theta) \right]^2 = \sum_{\omega_1 \in \Omega} \frac{[S'(\omega_1)]^2}{S^2(\omega_1)} + o(N). \end{aligned}$$

Thus we have for $\gamma > 1$

$$\text{Var}\left\{ \sum_{\omega_1 \in \Omega} Y(\omega_1; \theta) \right\} = \sum_{\omega_1 \in \Omega} \frac{[S'(\omega_1)]^2}{S^2(\omega_1)} + o(N) = - \sum_{\omega} \mathbb{E} \frac{d^2}{d^2\theta} Y(\omega) + o(N). \quad (5.1)$$

The covariances of frequency contributions to either the score or the Fisher information behave in this fashion. Thus the observed Fisher information converges to the expected Fisher information. As long as the correlation is decaying sufficiently rapidly, then we can mainly ignore the blurring causing frequency correlation.

To show typical spread of correlation of the Fourier transform we refer to Figure 2, which substantiates this view, showing weak correlations between frequencies for typical Matérn processes, unless the spectrum is extremely variable compared to the sample size (corresponding to a large η value). Such effects are similar to the case of bias from leakage, but the consequences of the effects are different. The bias of the periodogram has a stronger and a more immediate effect on the spectral estimates than the correlation because any perturbation away from zero will cause a consistent bias of the parameter estimates. The Fisher matrix is normally less affected by the blurring. This is because its expectation will be dominated by its non-zero mean, and its variance has only manageable inflation, as is clarified by equation (5.1). This is our argument for why it is sensible to blur the spectrum to correctly specify its expectation, but why we do not to take account of the correlation. As we expect the interactions between the true spectrum and the Féjer kernel to have limited spread in frequency, this is reasonable. By using the blurred Whittle likelihood, to account for the spectral blurring of the periodogram, this allows us to compromise between computational tractability, and to still achieve good statistical properties.

6 Inference for Complex-Valued Time Series

6.1 Semi-parametric inference

As discussed in Section 4.1, the frequencies included in the summation of the Whittle likelihood in equations (4.3) and (4.4) can be performed over a reduced range of frequencies Ω , such that inference is semi-parametric. We note work by Robinson (1995), and similar papers by this author, which also perform frequency-domain inference semi-parametrically. In contrast to our work, his approach is aimed for inferring long-memory processes such as fractional Brownian motion and moreover, in his procedure there is no bias-correction performed in the Whittle Likelihood, as we have proposed in equation (4.4).

There are essentially two reasons to perform semi-parametric inference in the way we have defined. The first is in the instance that a model is only correctly specified within a certain range of frequencies. For example, in Lumpkin and Elipot (2010), the movement of surface drifter pairs exhibit different spectral slopes for certain ranges of frequencies. If we are just interested in inferring parameters of one of the slopes, then this can be performed semi-parametrically by constraining Ω accordingly.

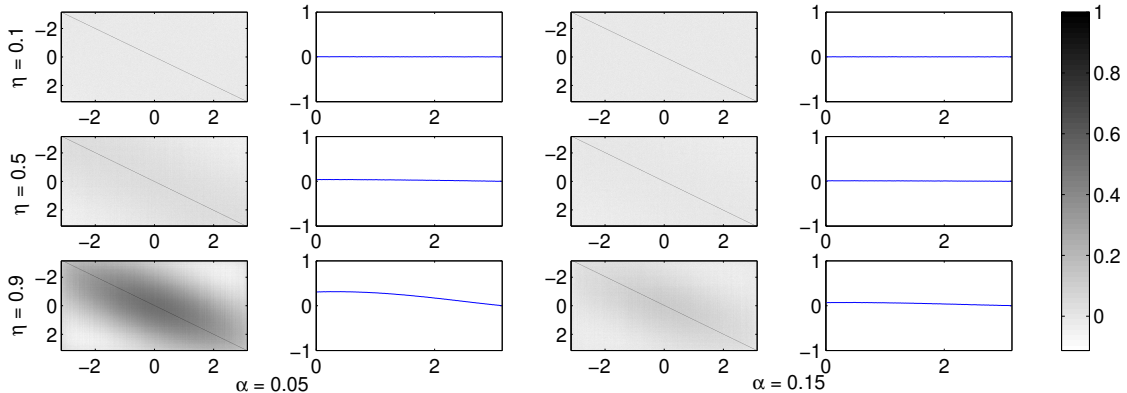


Figure 2: Correlations between the Fourier transform (real component only) at each pair of Fourier frequencies $\omega\Delta \in [-\pi, \pi]$ (left) and for each distance between Fourier frequencies in the interval $\omega\Delta \in [0, \pi]$ (right), for different Matérn processes each of length 500, averaged over 1,000 repeats.

The second reason to constrain Ω is when the regularly sampled process is obtained from irregularly sampled *raw* data by interpolation. The interpolation is required for frequency-domain analysis to work as the discrete Fourier transform requires regularly sampled data, but the resulting spectrum can be markedly affected by the method of interpolation used, particularly at high frequencies where energy is usually underestimated. This can lead to biased parameter estimates for the underlying continuous model. In such cases, a model for the distribution of time-intervals between observations in the raw data could be applied to *degrade* the data, such that interpolation effects are correctly accounted for. Such models are not always available, however, and even if they are, the implementation can cause considerable computational burden.

As a result, there is an apparent intermediate solution, which is to constrain Ω such that high-frequencies are removed from estimation. If the sampling periods are *almost* regular, then Ω can still be permitted to extend close to the Nyquist frequency. In any case, the appropriate cut-off for Ω can often be conservatively selected by looking at $\max(\Delta_t)$ or hand-picked by analysing the spectrum – as in the case of Figure 1 for oceanographic drifter data, where only frequencies greater than $\omega\Delta > 2$ appear to be affected by interpolation. Semi-parametric inferences must therefore be implemented carefully, to ensure a correct specification of degrees of freedom.

Finally, if the rotary components are shown to be uncorrelated (by testing for propriety as discussed in Section 6.2) then we can estimate parameters of one of Z^+ or Z^- by analysing one-side of the spectrum only, and then using the form of the Whittle likelihood given in either equation (4.3) or (4.4), replacing X for Z^+ or Z^- , although we prefer to use both sides of the spectrum if they are not contaminated, to minimise the variance of our estimates.

6.2 Hypothesis testing for impropriety

In Sections 3.1 and 3.2 we defined the coherence between components of a complex-valued time series, in particular, between the rotary components Z^+ and Z^- . We may wish to test this model against the simpler scenario where $S_{+-}(\omega) = 0$ for all ω , as this model is preferable unless there is sufficient evidence to suggest something more complicated. This hypothesis corresponds to there being no linkage of the positive rotating and negative rotating phasors. We note from Section 3.2 that this hypothesis is *not* equivalent to $S_{XY}(\omega) = 0$ and that a process with a zero rotary cross-spectra ($S_{+-}(\omega) = 0$) is equivalent to a proper process ($R_{ZZ}(\omega) = 0$). This is a deliberate and convenient consequence of the way we have constructed Z^+ and Z^- to *both* be analytic. Testing for impropriety in the time-domain is then equivalent to testing for a non-zero cross-spectrum between rotary components in the frequency domain.

There have been many tests for impropriety using data sets of multiple replicates of complex-valued

vectors, see for example (Schreier and Scharf, 2010; Ollila and Koivunen, 2004). We note, however, that these are *non-parametric tests* using replicated complex-valued vectors. We have a simple *parametric* time series model suitable for a *single* time series, and will derive a test statistic for this scenario.

For example, we have proposed to study the Matérn model in Section 3.3, and can estimate suitable parameters for ϕ , ν and α by using the Whittle likelihood, which can also be permitted to differ across the Cartesian or rotary components as discussed. We can also estimate the coherence structure by specifying a model for $\sigma_{\pm}(\omega)$ and $\theta_{\pm}(\omega)$. We may however prefer to use the simpler model where $S_{+-}(\omega) = 0$ and we can make use of the parametric model – specifically the Whittle likelihood score – to perform a likelihood ratio test to check for evidence if $\rho_{\pm}(\omega) \neq 0$ (in equation (3.6)) such that $S_{+-}(\omega) = 0$. Specifically, this is done by computing the likelihood ratio statistic and therefore calculating

$$W = 2(\ell_t(\hat{\boldsymbol{\theta}}_1^{(t)}) - \ell_t(\hat{\boldsymbol{\theta}}_0^{(t)})) \approx 2(\ell_f(\hat{\boldsymbol{\theta}}_1^{(f)}) - \ell_f(\hat{\boldsymbol{\theta}}_0^{(f)})),$$

where $\hat{\boldsymbol{\theta}}_1$ includes non-zero estimates for the coherency $\rho_{\pm}(\omega)$ (or $\rho_{XY}(\omega)$ for the Cartesian decomposition) and in the case of $\hat{\boldsymbol{\theta}}_0$, $\rho_{+-}(\omega)$ is set to 0 for all ω .

Following standard likelihood theory, the likelihood ratio statistic W is asymptotically distributed according to a χ^2 distribution with degrees of freedom equal to the number of extra parameters in the alternative hypothesis versus the null. In the case of the coherency structure proposed in equations (3.3) and (3.4), the degrees of freedom is equal to $r + l$, which in the case of a constant coefficient across frequencies with no group delay is equal to 1. We can then conduct hypothesis tests against the χ^2 distribution in the usual way to test for evidence of impropriety, such that the user can then contrast finding with non-parametric methods. We investigate this with examples in Section 7.2.

6.3 Model choice

In this paper we have so far assumed the distribution of the process and the corresponding number of unknown parameters is known *a priori*. In many instances this will not be the case. When a number of possible candidates for the process are nested, such as a range of ARMA(p, q) processes, then the Akaike Information Criterion (AIC) can be used to find the most appropriate choice of p and q . Similarly, model choice can be used to select between a Matérn and fractional Brownian motion – as the spectrum of fractional Brownian motion is nested functionally (but not formally) inside that of a Matérn (by setting $\alpha = 0$ in equation (3.8)). Finally model choice can also be used to check if certain parameter values are correctly known *a priori*, such as the slope parameter ν , which is assumed for physical reasons to be a fixed known value for certain oceanographic time series (as in Lumpkin and Elipot (2010)). The AIC can be closely-approximated in the frequency-domain using the Whittle likelihood. This is done by using the Whittle likelihood to approximate the time-domain likelihood and combining this with choices of model-penalisation as in Hurvich and Tsai (1989):

$$\text{AIC}(\hat{\boldsymbol{\theta}}^{(t)}) = -2\ell_t(\hat{\boldsymbol{\theta}}^{(t)}) + 2p \approx -2\ell_f(\hat{\boldsymbol{\theta}}^{(f)}) + 2p,$$

where p is the number of parameters in the model. The model with the smallest AIC value is then selected. The AIC therefore selects the most parsimonious model, unless there is sufficient evidence to suggest (through an increased likelihood score) that extra parameters should be used. For small sample-sizes, it is often recommended to use a correction to the AIC known as the AICC, which for complex-valued time series is given by

$$\text{AICC}(\hat{\boldsymbol{\theta}}^{(t)}) = -2\ell_t(\hat{\boldsymbol{\theta}}^{(t)}) + \frac{4pN}{2N - p - 1} \approx -2\ell_f(\hat{\boldsymbol{\theta}}^{(f)}) + \frac{4pN}{2N - p - 1}, \quad (6.1)$$

which in any case converges to the AIC for large sample-sizes. The correction uses $2N$ (rather than N as would be done for real-valued time series) as there are $2N$ degrees-of-freedom in a length N complex-valued time series. In the case of semi-parametric estimation, equation (6.1) should not be used, as the sample-size correction needs to take account of degrees-of-freedom in the data not used in the estimation. We instead replace N by $N_{\mathcal{J}}$ in equation (6.1), which is the number of Fourier frequencies used in the frequency range

Ω in the Whittle-likelihood estimation. Care must be taken when between real-valued and complex-valued time series, as the degrees of freedom behave the same at any given frequency, but for complex-valued series there are twice as many frequencies to consider.

We note that if a tapered version of the spectrum is used in Whittle likelihood estimation, then the degrees-of-freedom are further reduced by the correlation induced in neighbouring Fourier frequencies by the taper. Without tapering, nominally every observation spaced $1/(N\Delta)$ are uncorrelated. With tapering every observation spaced $c/(N\Delta)$ is uncorrelated. We must then further reduce $N_{\mathcal{J}}$ by a factor of c in the AICC, which can be computed by Fourier transforming the taper onto a fine grid and then finding the frequency width where the transformed sequence is only correlated below some threshold (such as 0.05).

Finally, model choice can also be used to select appropriate models for the coherence (see for example equations (3.3) and (3.4)) but a likelihood ratio test is perhaps better in the first instance as the asymptotic distributional form of the likelihood can be used to make stronger statements on the existence of a non-zero coherence structure, after which – if the null is rejected – model choice can be used to help determine an appropriate model.

7 Examples and Simulations

7.1 The Blurred Whittle Likelihood

In Chapter 4, we discussed several frequency-domain approximations to the standard time-domain maximum likelihood, and advocated the use of the blurred Whittle likelihood ($\ell_f(\boldsymbol{\theta})$ in equation (4.4)) or the tapered blurred Whittle likelihood ($\ell_{hf}(\boldsymbol{\theta})$ in equation (4.7)) which closely approximates the time-domain likelihood in a computationally efficient manner, by taking account of blurring and aliasing effects in the discrete Fourier transform. In this section we demonstrate the effectiveness of blurring the Whittle likelihood in a Monte Carlo study using data simulated from the Matérn process and then compare the parameter estimates for each type of likelihood.

We set our parameter values to be equal to those typically found for surface drifter trajectories ($A = 10, \nu = 0.4, \alpha = 0.05$ in equation (3.8)) which would be a good fit to the time-windowed spectra displayed in Figure 1 (excluding the two peaks representing other oscillatory oceanographic processes). Tables 1 and 2 display the results of our Monte Carlo study for $N = 250$ and $N = 1,000$ respectively, where in each case we have averaged over 10,000 repeats to remove sampling variability. Note that we include results for two tapers – a discrete prolate spheroidal sequence taper (of order zero, see Percival and Walden (1993)) and a full cosine taper (Velasco and Robinson, 2000) – where the latter addresses leakage effects most drastically. For standard Whittle estimators we also need to fold in aliased frequencies (for continuous sampled process) to find the spectrum, which does not have an analytic form for the Matérn process for example (c.f. equation (3.8)), and must be instead computed numerically. We consider two such approximations, with $k = 10$ and $k = 50$, which correspond to the number of adjacent frequencies (at intervals of 2π) folded into the spectrum for the likelihood. The choices of the time series length N are similar to the simulation comparison performed in Velasco and Robinson (2000) (200 and 512) and also correspond to a reasonable range of observations used as a window for oceanographic data assuming local stationarity (corresponding to approximately 20-80 days of ocean drifter measurements) – shorter time series are too variable and longer time series typically correspond to drifters that visit new spatial areas with different characteristics.

The time-domain estimator performs the best, as expected, but at a considerable computational expense, where the optimisation is two orders of magnitude slower. This is despite using the Cholesky decomposition to more efficiently compute the determinant *and* inverse of the covariance matrix (although this can lead to instability for small N). For large data sets, such as that collected from the Global Drifter Program, this burden is significant when computing across many million data points over rolling windows of time. In addition, for complex-valued time series, we may wish to specify rotary models in the frequency-domain, which are not at all easy to formulate in the time-domain, as improper models would need smoothing in their time domain specification, further increasing the computational burden.

Among the remaining frequency-domain estimators there are some initially counterintuitive results, such

Table 1: Average performance of different likelihood estimators with a Matérn process ($N = 250$)

Method	Eqn	$\sigma = 10$		$\nu = 0.4$		$\alpha = 0.05$		CPU time (seconds)
		Bias	RMSE	Bias	RMSE	Bias	RMSE	
time domain	(4.1)	.0279	.6167	.0060	.0530	.0121	.0367	21.9788
periodogram $k = 10$	(4.3)	.4051	.7982	-.0047	.0572	.0143	.0390	.1674
periodogram $k = 50$	(4.3)	.2925	.7654	.0078	.0550	.0165	.0403	.7956
blurred periodogram	(4.4)	.0234	.7284	.0062	.0559	.0128	.0389	.1684
dpss taper $k = 10$	(4.6)	.2194	.7121	-.0047	.0650	.0148	.0437	.1684
dpss taper $k = 50$	(4.6)	.1064	.7099	.0078	.0624	.0170	.0449	.7970
blurred dpss taper	(4.7)	.0432	.7176	.0081	.0621	.0164	.0448	.1782
cosine taper $k = 10$	(4.6)	.2332	.8708	.0005	.0803	.0222	.0584	.1686
cosine taper $k = 50$	(4.6)	.1210	.8774	.0129	.0779	.0244	.0598	.7971
blurred cosine taper	(4.7)	.0654	.8924	.0122	.0776	.0237	.0598	.1786

Table 2: Average performance of different likelihood estimators with a Matérn process ($N = 1000$)

Method	Eqn	$\sigma = 10$		$\nu = 0.4$		$\alpha = 0.05$		CPU time (seconds)
		Bias	RMSE	Bias	RMSE	Bias	RMSE	
time domain	(4.1)	.0044	.2959	.0014	.0252	.0029	.0151	223.6258
periodogram $k = 10$	(4.3)	.1986	.3576	-.0122	.0297	.0016	.0149	.4097
periodogram $k = 50$	(4.3)	.0845	.3184	.0002	.0258	.0037	.0155	3.0641
blurred periodogram	(4.4)	.0033	.3117	.0014	.0256	.0030	.0154	.3987
dpss taper $k = 10$	(4.6)	.1472	.3591	-.0123	.0336	.0018	.0172	.4096
dpss taper $k = 50$	(4.6)	.0329	.3409	.0001	.0298	.0039	.0178	3.0649
blurred dpss taper	(4.7)	.0063	.3434	.0021	.0294	.0041	.0179	.4061
cosine taper $k = 10$	(4.6)	.1466	.4233	-.0113	.0396	.0036	.0179	.4073
cosine taper $k = 50$	(4.6)	.0325	.4126	.0012	.0362	.0057	.0216	3.0469
blurred cosine taper	(4.7)	.0113	.4164	.0032	.0357	.0060	.0223	.4047

as folding in fewer frequencies in the likelihood performing better for certain parameters (but not all). This is due to the finite sample bias and variance characteristics of the spectrum off-setting each other at times. It is generally the case that blurring the likelihood improves the accuracy of parameter estimates – particularly for periodogram based methods. The improvement with tapering is less noticeable however, although this is not so surprising as leakage effects are largely accounted for and additional blurring is therefore not as important. The other key reason to blur however (for *both* periodograms and tapers), is that this efficiently takes account of aliasing effects. This approach is much more computationally efficient than folding in the required number of aliased frequencies in the non-blurred spectrum, particularly if the slope parameter is small. Folding in 10 adjacent sets of frequencies is already as computationally intensive as blurring, and for these parameters the difference between the estimates with $k = 10$ and $k = 50$ is marked. Periodogram estimators perform better than tapered estimators in this study in general, but we note that increasing the slope parameter ν leads to a higher dynamic range in the spectrum, sometimes rendering tapered methods suitable (Velasco and Robinson, 2000).

7.2 Rotary Modelling of Oceanographic Processes

In this section we show the advantages of modelling bivariate processes in terms of their rotary decomposition. Specifically we track the spatial trajectories of particles over time from two sets of numerical experiments, snapshots of which are displayed in Figure 3. In these simulations, the particle trajectories are computed from a two-dimensional turbulent fluid simulation using the barotropic potential vorticity equation under both isotropic (f -plane) and anisotropic (β -plane) dynamics, as described in Vallis (2006). Both the presence of anisotropy in the trajectories, and the time scale associated with these anisotropies are of interest. Because

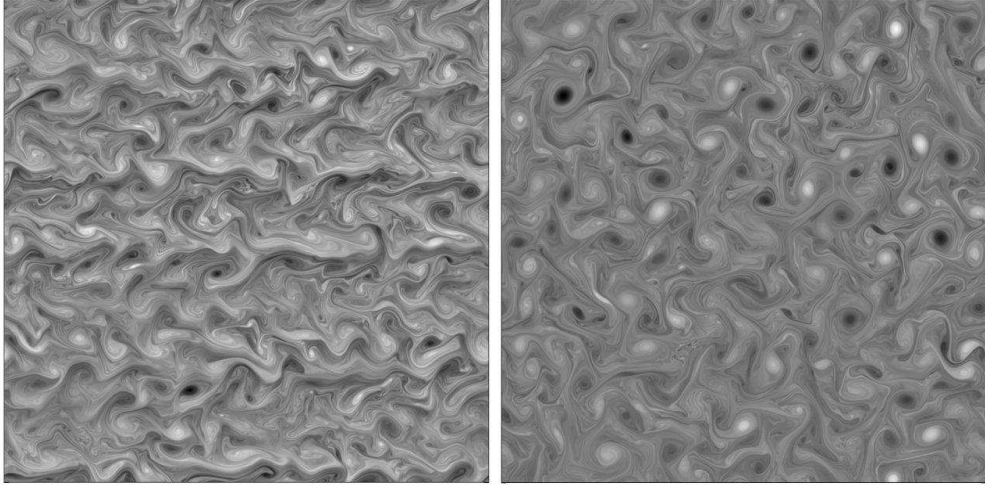


Figure 3: Snapshot of the relative vorticity field on the last day of the simulation for the anisotropic (left) and isotropic (right) fluid simulation.

the data was simulated, we can assess which frequencies are associated with the anisotropic behaviour, from the settings of the numerical model. This can be calculated using the Rhines scale (Rhines, 1975) which is found by comparing the root mean square velocity of the fluid to the Rossby wave phase speed. For the simulations here, this time is approximately 23 days for the anisotropic experiment.

We can model the velocities of the trajectories as Lagrangian time series that follow a Matérn processes, and take account of anisotropy by modelling the rotary coherency using the following 1-parameter model:

$$\sigma_{\pm}(\omega) = \max(0, 1 - c|\omega\Delta|). \quad (7.1)$$

This simple model naturally defines a timescale at which anisotropy begins, as the coherence is zero at $\omega = 1/c\Delta$, corresponding to timescales of $2\pi c\Delta$, and then increases linearly (with respect to the spectrum) until at long timescales all energy is considered to be in the dominant Cartesian component. Equation (7.1) then defines the rotary cross-spectrum and should be correctly blurred, together with the spectrum of the Matérn process, as discussed already in Section 4. The appropriateness of the fit is displayed in Figure 4 for the anisotropic data, where we have used a semi-parametric fit by excluding half the frequencies ($\omega\Delta > \pi/2 = \Omega_{\max}$) and also excluding the zero frequency as we cannot estimate $\rho_{+-}(\omega)$ here. The extra parameter has succinctly captured the difference between the flow in each Cartesian component at low frequencies, which corresponds to an increased likelihood score for such a model as compared with the simpler isotropic fit ($\theta_{\pm}(\omega) = 0$) – the Matérn process is also a good fit for the complex-valued trajectories.

To put our choice of model under further scrutiny, we fit the anisotropic model to 248 trajectories from the anisotropic experiment (of length 1001) and compare the likelihood score versus the null hypothesis of an isotropic model. We can then use a likelihood ratio test as described in Section 6.2 to test for evidence of anisotropy. For consistency, we also repeat this procedure with the same number of trajectories (of the same length) from the isotropic experiment in Figure 3 (right) and see if we correctly do not reject the null in such cases. The set of likelihood ratio test statistics from both experiments is displayed in Figure 5 (left). The statistics are compared with the 95% one-sided confidence interval for the χ_1^2 distribution (as there is only 1 additional parameter in the alternate) and we can see that the isotropic model is correctly always rejected for the anisotropic data and rejected only 12 times for the isotropic model – which is in agreement with a type I error level set to 5%. In experimental rather than controlled data we would account for multiple testing issues if performing this test over multiple trials, and apply a technique such as False Discovery rates. Figure 5 (right) displays the spread of estimates for $2\pi c\Delta$ which gives us an estimate of the timescale at which anisotropy begins. Interestingly the estimated time scale has not yet converged to

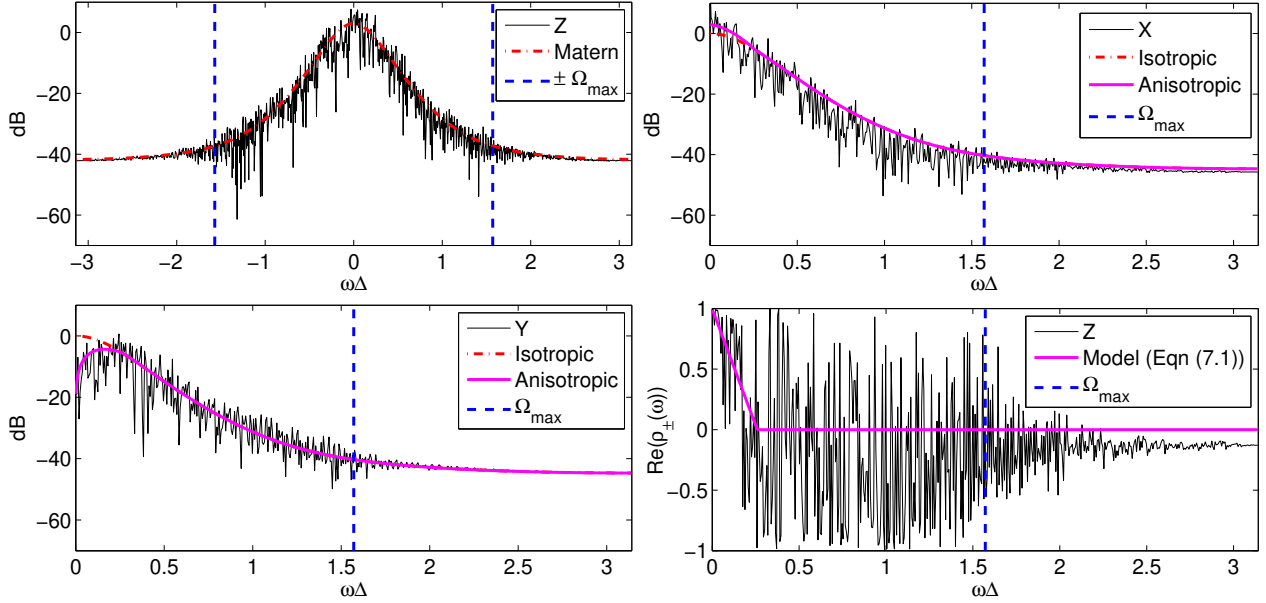


Figure 4: Isotropic and Anisotropic fits using the Matérn process for an anisotropic trajectory.

a Gaussian distribution, probably because of the natural truncation of its model type. In the numerical experiment this is set at approximately 23 days and this is consistent with most of the estimates from the trajectories (the median in the figure is 24.7 days). The rotary modelling techniques we have developed are therefore a powerful tool for capturing and quantifying physical structure in complex-valued processes.

8 Conclusions

In this paper we have introduced how Whittle estimation is implemented for parametric complex-valued time series. We have shown the value of separating out different frequency behaviour and providing a model for the ranges of frequencies separately. This permitted us to handle a plethora of different effects directly in the frequency domain, and introduce new parametric model characteristics. For example, we demonstrated how our techniques can be used to effectively capture anisotropy in oceanographic flow models.

Importantly for small samples we proposed the usage of the blurred Whittle likelihood. This allowed us to significantly reduce bias, whilst still keeping computations relatively efficient, as evidenced in a Monte Carlo study. This combined with good frequency domain models for the spectrum yielded flexible, yet parsimonious models for oceanographic time series. These models yield insight into how we should think about complex-valued time series, and how random ellipses at every frequency combine to form a model for temporal dependence.

There are significant challenges remaining both for the study of oceanographic and complex-valued time series. Most importantly we need to develop and understand further flexibly structured behaviour that introduces nontrivial relationships. Oceanographic data can be highly heterogeneous, and so we need to iteratively understand more and more of the structure found in such data. Primarily we wish to isolate main structure in the variance of the Fourier transform. It would be naïve to assume that all structure of the data can be found in this variance, and once we have calculated residuals from the data, subsequent features can be used to discover any remaining structure. The area is also quite fortunate in having both physical data, combined with highly accurate and sophisticated models. Once both sources of patterned behaviour are understood, then we can use this understanding to inform global circulation and climate modelling in general.

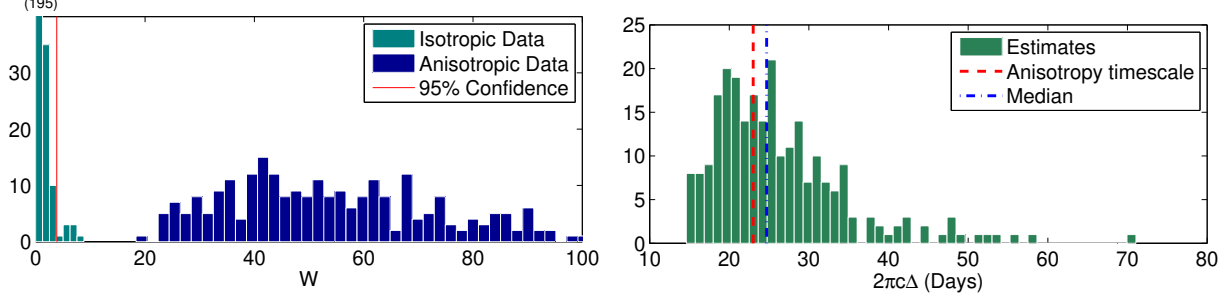


Figure 5: Testing for isotropy (left) and the anisotropy timescale (right).

A The bivariate Matérn process

Gneiting et al. (2010) prove that the necessary *and* sufficient conditions for a bivariate ($p = 2$) Matérn process, with Matérn cross-covariances, are

$$\rho_{12}^2 \leq \frac{\Gamma(\nu_1 + 1)}{\Gamma(\nu_1)} \frac{\Gamma(\nu_2 + 1)}{\Gamma(\nu_2)} \frac{\Gamma(\nu_{12})^2}{\Gamma(\nu_{12} + 1)^2} \frac{\alpha_1^{2\nu_1} \alpha_2^{2\nu_2}}{\alpha_{12}^{4\nu_{12}}} \inf_{t \geq 0} \frac{(\alpha_{12}^2 + t^2)^{2\nu_{12} + 2}}{(\alpha_1^2 + t^2)^{\nu_1 + 1} (\alpha_2^2 + t^2)^{\nu_2 + 1}}.$$

where in the case $\alpha_1 = \alpha_2 = \alpha_{12}$ and $\nu_{12} = \frac{1}{2}(\nu_1 + \nu_2)$ this condition simplifies to

$$|\rho_{12}| \leq \frac{\Gamma(\nu_1 + \frac{1}{2})^{1/2}}{\Gamma(\nu_1)^{1/2}} \frac{\Gamma(\nu_2 + \frac{1}{2})^{1/2}}{\Gamma(\nu_2)^{1/2}} \frac{\Gamma(\frac{1}{2}(\nu_1 + \nu_2))}{\Gamma(\frac{1}{2}(\nu_1 + \nu_2) + \frac{1}{2})}. \quad (\text{A.1})$$

At first glance this condition appears to suggest that our bivariate specification in equation (3.1) does not permit a full bivariate Matérn for all constant $0 \leq \rho_{XY} \leq 1$ for certain values of ν_X and ν_Y . This is because of the different normalisation of the Matérn with different parameter values (compare equation (3.7) in this paper with equation (1) in Gneiting et al. (2010)), meaning restrictions on the correlation coefficient ρ_{XY} and ρ_{12} are *not* identical. To overcome this we consider the spectrum of the Gneiting et al. (2010) representation:

$$S_1(\omega) = \frac{\phi_1^2 \left(\frac{\alpha^{2\nu_1}}{\pi^{1/2}} \frac{\Gamma(\nu_1 + 1/2)}{\Gamma(\nu_1)} \right)}{(\omega^2 + \alpha^2)^{\nu_1 + 1/2}},$$

and similarly for $S_2(\omega)$. We then note that:

$$\begin{aligned} (S_1 S_2)^{1/2} &= \left(\frac{\phi_1^2 \left(\frac{\alpha^{2\nu_1}}{\pi^{1/2}} \frac{\Gamma(\nu_1 + 1/2)}{\Gamma(\nu_1)} \right)}{(\omega^2 + \alpha^2)^{\nu_1 + 1/2}} \frac{\phi_2^2 \left(\frac{\alpha^{2\nu_2}}{\pi^{1/2}} \frac{\Gamma(\nu_2 + 1/2)}{\Gamma(\nu_2)} \right)}{(\omega^2 + \alpha^2)^{\nu_2 + 1/2}} \right)^{1/2} \\ &= \frac{\phi_1 \phi_2 \frac{\alpha^{\nu_1 + \nu_2}}{\pi^{1/2}} \frac{\Gamma(\nu_1 + \frac{1}{2})^{1/2}}{\Gamma(\nu_1)^{1/2}} \frac{\Gamma(\nu_2 + \frac{1}{2})^{1/2}}{\Gamma(\nu_2)^{1/2}}}{(\omega^2 + \alpha^2)^{1/2(\nu_1 + \nu_2) + 1/2}} \\ &= \frac{\Gamma(\nu_1 + \frac{1}{2})^{1/2}}{\Gamma(\nu_1)^{1/2}} \frac{\Gamma(\nu_2 + \frac{1}{2})^{1/2}}{\Gamma(\nu_2)^{1/2}} \frac{\Gamma(\frac{1}{2}(\nu_1 + \nu_2))}{\Gamma(\frac{1}{2}(\nu_1 + \nu_2) + \frac{1}{2})} \frac{\phi_1 \phi_2 \frac{\alpha^{2[1/2(\nu_1 + \nu_2)]}}{\pi^{1/2}} \frac{\Gamma(\frac{1}{2}(\nu_1 + \nu_2) + \frac{1}{2})}{\Gamma(\frac{1}{2}(\nu_1 + \nu_2))}}{(\omega^2 + \alpha^2)^{1/2(\nu_1 + \nu_2) + 1/2}} \\ &= \frac{\Gamma(\nu_1 + \frac{1}{2})^{1/2}}{\Gamma(\nu_1)^{1/2}} \frac{\Gamma(\nu_2 + \frac{1}{2})^{1/2}}{\Gamma(\nu_2)^{1/2}} \frac{\Gamma(\frac{1}{2}(\nu_1 + \nu_2))}{\Gamma(\frac{1}{2}(\nu_1 + \nu_2) + \frac{1}{2})} S_{12}(\omega). \end{aligned}$$

This implies that

$$\rho_{12} = \left[\frac{\Gamma(\nu_1 + \frac{1}{2})^{1/2}}{\Gamma(\nu_1)^{1/2}} \frac{\Gamma(\nu_2 + \frac{1}{2})^{1/2}}{\Gamma(\nu_2)^{1/2}} \frac{\Gamma(\frac{1}{2}(\nu_1 + \nu_2))}{\Gamma(\frac{1}{2}(\nu_1 + \nu_2) + \frac{1}{2})} \right] \rho_{XY},$$

and the condition in equation (A.1) simplifies to: $|\rho_{XY}| \leq 1$, as required to show that the condition $\alpha_X = \alpha_Y$ defines a full bivariate Matérn as defined by Gneiting et al. (2010), and similarly for $\alpha_+ = \alpha_-$ in the complex-valued case.

References

- Apanasovich, T. V., M. G. Genton, and Y. Sun (2012). A valid Matérn class of cross-covariance functions for multivariate random fields with any number of components. *J. American Statistical Association* 107(497), 180–193.
- Bloomfield, P. (2004). *Fourier analysis of time series: an introduction*. Wiley.
- Dahlhaus, R. (1988). Small sample effects in time series analysis: A new asymptotic theory and a new estimate. *The Annals of Statistics* 16, 808–841.
- Davis, R. E., R. DeSzoeko, and P. Niiler (1981). Variability in the upper ocean during MILE. part II: Modeling the mixed layer response. *Deep Sea Res.* 28(12), 1453–1475.
- Dzhaparidze, K. O. and A. M. Yaglom (1983). Spectrum parameter estimation in time series analysis. *Developments in statistics* 4, 1–96.
- Gneiting, T., W. Kleiber, and M. Schlather (2010). Matérn cross-covariance functions for multivariate random fields. *JASA* 105(491), 1167–1177.
- Gonella, J. (1972). A rotary-component method for analysing meteorological and oceanographic vector time series. *Deep Sea Res.* 19, 833–846.
- Griffa, A., A. D. Kirwan Jr, A. J. Mariano, T. Özgökmen, and T. Rossby (2007). *Lagrangian analysis and prediction of coastal and ocean dynamics*. Cambridge University Press.
- Hamon, B. V. and E. J. Hannan (1974). Spectral estimation of time delay for dispersive and non-dispersive systems. *Applied Statistics* 23, 134–142.
- Hansen, D. V. and P.-M. Poulain (1996). Quality control and interpolations of WOCE/TOGA drifter data. *J. Atmospheric & Oceanic Technology* 13, 900–910.
- Hindberg, H. and A. Hanssen (2007). Generalized spectral coherences for complex-valued harmonizable processes. *IEEE Trans. Signal Processing* 55, 2407–2413.
- Hurvich, C. M. and C. L. Tsai (1989). Regression and time series model selection in small samples. *Biometrika* 76(2), 297–307.
- LaCasce, J. H. (2008). Statistics from Lagrangian observations. *Progress in Oceanography* 77(1), 1–29.
- Lumpkin, R. and S. Elipot (2010). Surface drifter pair spreading in the north atlantic. *J. Geophysical Res.* 115(C12), C12017.
- Olhede, S. C. (2006). On probability density functions for complex variables. *IEEE Trans. Information Theory* 52, 1212–1217.
- Olhede, S. C. and A. T. Walden (2003). Noise reduction in directional signals using multiple morse wavelets illustrated on quadrature doppler ultrasound. *IEEE Trans. Biomedical Engineering* 50(1), 51–57.
- Olhede, S. C. and A. T. Walden (2004). Analytic wavelet thresholding. *Biometrika* 91, 955–973.
- Ollila, E. and V. Koivunen (2004). Generalized complex elliptical distributions. *IEEE Sensor Array and Multichannel Signal Processing Workshop Proceedings*, 460–464.

- Percival, D. B. and A. T. Walden (1993). *Spectral Analysis for Physical Applications*. Cambridge University Press.
- Percival, D. B. and A. T. Walden (2006). *Wavelet methods for time series analysis*, Volume 4. Cambridge University Press.
- Rhines, P. B. (1975). Waves and turbulence on a beta-plane. *J. Fluid Mechanics* 69(3), 417–443.
- Robinson, P. M. (1995). Gaussian semiparametric estimation of long range dependence. *The Annals of statistics* 23(5), 1630–1661.
- Rowe, D. B. (2005). Modeling both the magnitude and phase of complex-valued fmri data. *NeuroImage* 25(4), 1310–1324.
- Rubin-Delanchy, P. and A. Walden (2008). Kinematics of complex-valued time series. *IEEE Trans. Signal Processing* 56(9), 4189–4198.
- Schreier, P. J. and L. L. Scharf (2010). *Statistical signal processing of complex-valued data: the theory of improper and noncircular signals*. Cambridge University Press.
- Thomson, D. J. (1990). Quadratic-inverse spectrum estimates: applications to palaeoclimatology. *Phil. Trans. Physical Sciences and Engineering* 332, 539–597.
- Vallis, G. K. (2006). *Atmospheric and oceanic fluid dynamics: fundamentals and large-scale circulation*. Cambridge University Press.
- Van Bellegem, S. and R. Dahlhaus (2006). Semiparametric estimation by model selection for locally stationary processes. *J. Royal Statistical Society: Series B* 68(5), 721–746.
- Velasco, C. and P. M. Robinson (2000). Whittle pseudo-maximum likelihood estimation for nonstationary time series. *J. American Statistical Association* 95, 1229–1243.
- Wahba, G. (1971). Some tests of independence for stationary multivariate time series. *J. Royal Statistical Society: Series B* 33, 153–166.
- Walden, A. T. (2013). Rotary components, random ellipses and polarization: a statistical perspective. *Phil. Trans. of the Royal Society A* 371, 20110554.
- Whittle, P. (1953a). The analysis of multiple stationary time series. *J. Royal Statistical Society: Series B* 15, 125–139.
- Whittle, P. (1953b). Estimation and information in stationary time series. *Arkiv for Matematik* 2, 423–434.